THE UNIVERSITY
of EDINBURGH

Dimensionality reduction for EMG prediction of upper-limb activity in freely-behaving primates

Agamemnon Krasoulis

Master of Science by Research
Institute for Adaptive and Neural Computation
School of Informatics
University of Edinburgh

2013

Abstract

Neural prosthetic systems aim to assist patients suffering from sensory, motor and other disabilities by translating neural brain activity into control signals for assistive devices, such as computers and robotics prostheses, or by restoring muscle contraction through functional electrical stimulation (FES). In a neuro-motor prosthetic device, the prediction of intended muscle activity is required for effective FES. It has been already known that upper-limb electromyogram (EMG) signals in primates, can be accurately predicted during repetitive tasks, by decoding the spiking-activity (SA) of single cells and multi-unit activity (MUA) in the motor cortical areas. Recent work now suggests that EMG signals can also be decoded by local field potential (LFP) recordings from the same areas. In such decoding schemes, the number of input variables is usually very large and no systematic way of performing effective variable selection has yet been suggested. In this work, we demonstrated for the first time that muscle activity decoding from SA and LFP signals in the primary motor cortex (M1) and the ventral premotor cortex (PMv) areas is feasible during naturalistic free behaviour, and we compared the decoding performance of spike-, LFP- and hybrid decoders. We also tested the relative information in a number of LFP frequency bands, and found that mid-high and high-frequency bands ($70 - 244$ Hz) conveyed the most EMG-related information. Finally, we compared the decoding performance of a group of sparse regression algorithms, and we showed that a method based on the variational bayes (VB) outperformed the conventional Wiener cascade filter for LFP-decoders in the case of limited amount of training data. For longer training datasets, the results from all methods were comparable.

Acknowledgements

The completion and success of any research project depends largely on the joint contribution of many individuals. I would like to take this opportunity to express my gratitude to all those who made this dissertation possible.

First and foremost, I would like to thank my supervisor Dr. Kianoush Nazarpour, for his invaluable support and inspiration. Without his guidance and persistent help, this dissertation would have never been completed.

I would also like to express my gratitude to my co-supervisor Prof. Sethu Vijayakumar for his guidance, useful advice and the fruitful discussions we had on the progress of this project.

Special thanks goes to Dr. Andrew Jackson and Dr. Thomas E. Hall from the Institute of Neuroscience, University of Newcastle, for kindly sharing with us their experimental data. Neuroscience research relies heavily on data collection, which can be a time-consuming and expensive process, both in financial and ethical terms. Personally, I envisage an 'open-data' research community and, as such, I owe my deepest appreciation to scientists who turn this idea into practice.

I would also like to express my gratitude to the DTC Executive Committee for offering me the flexibility to work on a research project that I was really interested in.

Last but not least, I am grateful to the members of my family, Constantinos, Mirella, Karolina and Kaiti, for their encouragement and spiritual support throughout my academic life, as well as to my partner Ersi, to whom this dissertation is dedicated, for her endless love and support in all aspects of my life.

Declaration

I declare that this thesis was composed by myself, that the work contained herein is my own except where explicitly stated otherwise in the text, and that this work has not been submitted for any other degree or professional qualification except as specified.

(*Agamemnon Krasoulis*)

To Ersi

Table of Contents

List of Figures

List of Tables

Chapter 1

Introduction

In this introductory chapter, we provide a brief background on brain-machine interfaces (BMIs) for motor rehabilitation, and the different type of source signals used to decode muscle activity and kinematic parameters. We then indicate the major contributions of our study and, at the end of the chapter, we provide an outline of the rest of this thesis.

1.1 BMIs for motor rehabilitation

Electrical activity of neurons in the primary motor cortex (M1) has been found to correlate with both kinematic (e.g. position and velocity) (A. P. Georgopoulos, J. F. Kalaska, R. Caminiti, J. T. Massey, 1982), and kinetic (e.g. force) (Evarts, 1968) aspects of movement. These findings along with the clinical need for movement restoration after amputation or injury to the spinal cord have led to the development of BMIs which by recording activity from the M1 allow the users to move computer cursors (Serruya et al., 2002; Carmena et al., 2003; Hochberg et al., 2006) or robotic limbs (Velliste et al., 2008). In laboratory experiments, muscle contraction of temporarily paralysed animals has been achieved through functional electrical stimulation (FES) (Moritz et al., 2008; Ethier et al., 2012), and was found to be effective in allowing subjects to regain control of basic hand movements. Worldwide, thousands of people suffering from spinal cord injury (SCI), brainstem strokes or other disorders, would potentially benefit from a neuro-motor prosthesis (NMP) (Hochberg et al., 2006).

The operation of a NMP can be divided into four major components; signal acquisition, signal/information processing, neural decoding and control signal generation for artificial limb movement. The greatest challenge the NMP community will probably

have to face in the future is the ability to implement a clinically viable and compact prosthetic device, where signal acquisition and processing are being performed within a restrictive power budget (Linderman et al., 2008). However, the standards for decoding performance should retain a high priority, even within any physical (i.e. size) and power restrictions.

1.1.1 Source signals for BMIs

Most chronic BMI studies so far (Carmena et al., 2003; Hochberg et al., 2006; Pohlmeyer et al., 2007; Hochberg et al., 2012; Gilja et al., 2012; Ethier et al., 2012; Collinger et al., 2013), have used multielectrode arrays to record single spiking-activity (SA) or multi-unit activity (MUA), in order to decode movement-related information. Motion-related SA has been found to be present in the M1 even after three years of SCI (Hochberg et al., 2006). For effective FES, an accurate mechanism for prediction of electrical activity of muscles (i.e. electromyogram (EMG) signals) is needed, and many methods spanning from linear (Carmena et al., 2003), Wiener cascade filters (Pohlmeyer et al., 2007) and Kalman filters (Wu et al., 2006, 2009; Nazarpour et al., 2012) have been proposed in the literature.

Recently, it has been proposed that local field potential (LFP) signals recorded from motor cortical areas can be used to decode reach target location (Mehring et al., 2003; Flint et al., 2012b), movement direction (Rickert et al., 2005; Stark and Abeles, 2007), grasp type (Stark and Abeles, 2007; Spinks et al., 2008), kinematic parameters such as hand position and velocity (Zhuang et al., 2010; Bansal et al., 2011, 2012), and upper limb muscle activity (Flint et al., 2012a). Furthermore, LFP signals from the parietal reach region (PRR) (Scherberger et al., 2005; Hwang and Andersen, 2013), and the posterior parietal cortex (PPC) of primates (Asher et al., 2007), have been used to decode reach target location and movement direction.

Notably, it has been shown that the decoding performance of LFP signals is independent of the presence of SA recorded on the same electrodes (Flint et al., 2012b). The advantages of using LFPs instead of SA signals as source signals for BMIs are numerous; firstly, SA signals exhibit a large bandwidth, this being a result of the fast nature of action potentials. A commonly used sampling rate for SA is 30 kHz, which leads to high power requirements and thus increased heat and size of a potential prosthesis (Flint et al., 2012b). For LFP signals, however, the bandwidth is significantly lower (sampling rate at 1 kHz instead of 30 kHz for spike signals), which translates into lower power requirements for the NMP. Secondly, single-unit activity is difficult to record

for a long time after the implantation, this being due to various factors such as neurodegeneration and mechanical movements of the subject, and usually lasts only for a few months (Simeral et al., 2011).

Other signals which have been used for decoding kinematics of arm and muscle activity include electrocorticography (ECoG) signals (Schalk et al., 2007; Sanchez et al., 2008; Pistohl et al., 2008; Chao et al., 2010), and epidural field potentials (EFPs) (Slutzky et al., 2011; Shimoda et al., 2012). The latter method, by preserving the integrity of the dura, offers the advantage of lower risk of brain infection or subdural hemorrhage (Flint et al., 2012b).

1.2 Contribution of the study

1.2.1 EMG decoding during naturalistic free behaviour

Previous work on muscle activity decoding was mainly focused on predicting EMG signals during stereotypic and repetitive behaviour with limited variability across trials (Pohlmeyer et al., 2007; Nazarpour et al., 2012; Flint et al., 2012a; Shin et al., 2012). The first contribution of our study consists in decoding EMG activity in primates during naturalistic free behaviour. Some studies which have addressed this issue in the past (Bansal et al., 2011, 2012), were limited to decoding kinematic parameters, such as hand position and velocity. To the best of our knowledge, this is the first study to perform muscle activity decoding in primates during natural behaviour.

1.2.2 Dimensionality reduction for EMG decoding from LFP signals

For decoding EMG activity from LFP recordings, the LFP signals are usually decomposed into several frequency bands, the power in each band is computed, and subsequently used as an input to the decoder (Flint et al., 2012a). This yields a relatively large amount of input features, the exact number of which also depends on the filter length used for decoding. An effective way of performing feature selection is thus needed, in order to avoid overfitting situations, especially in the case of limited amount of training data. The second contribution of our study consists in systematically comparing a group of sparse regression algorithms, in terms of their performance in decoding EMG signals from spikes, LFPs, or a combination of these two types of signals (hybrid decoders).

1.3 Thesis outline

In this section, we present the basic structure of this thesis. The rest of this paper is organised as follows:

In **Chapter 2**, the basic background of this study is provided, and related work on the field is briefly presented. We mainly focus on muscle activity decoding from LFP signals, and methods used in the literature for feature selection in high-dimensional regression.

In **Chapter 3**, the methods used in this study are presented. We first describe the experimental and surgical procedures, and then explain in detail the implementation of the different types of decoders used in our study.

In **Chapter 4**, the results from our study are presented and discussed. Special focus is given on decoding from M1 and ventral premotor cortex (PMv) signals, the relative EMG-related information in different LFP frequency bands, and the decoding performance of the various sparse regression algorithms examined in this work.

Finally, **Chapter 5** summarises the key findings of our study, and some reflections on future research directions in the field are presented.

Appendices A, B and **C**, contain supplementary figures and results.

Chapter 2

Background and related work

In the first section of this chapter, we provide a brief review of previous work on the relationship between LFPs recorded in motor cortical and other brain areas, and movement-related information. In the second section, we present the methods proposed in the literature, for feature selection in decoding paradigms with cortical signals.

2.1 Decoding of movement-related information from LFP signals in primates

The cortical LFP has been thought as a summation signal of local excitatory and inhibitory synaptic potentials around the tip of the recording electrode. Spikes recorded from microelectrodes usually originate from large pyramidal cells, whereas LFP signals recorded on the same electrodes reflect the local synaptic activity. Therefore, LFPs are often thought to represent inputs and local processing activity in cells, whereas SA is thought to represent the output of cells' activity (Mitzdorf, 1987; Buzsáki, 2004).

Sanes and Donoghue (1993) were the first to study the correlation between movement and oscillatory activity in LFPs recorded from M1 in behaving monkeys, although they concluded that these oscillations were more strongly correlated with movement preparation, rather than execution. Murthy and Fetz (1996) later found correlations between LFP signals recorded in M1 and EMG signals recorded from forearm muscles.

Mehring et al. (2003) were the first to decode movement target and trajectories from LFPs in the motor cortex of monkeys, and they also showed that the decoding performance of a single LFP channel was comparable to that of the spike train of a single cell. Scherberger et al. (2005) were able to decode the animals' behavioural state (plan-

ning a reach or saccade), as well as direction of planned movement from single trial information, by recording LFP signals from PRR. Rickert et al. (2005) decomposed the LFP signals recorded in M1 of monkeys in 3 different bands, and subsequently performed movement direction decoding separately for each band. The best prediction was achieved by using the low-frequency (0-4 Hz) LFP band. Slightly different results were found by Heldman et al. (2006), who compared the correlation between arm position and the spectral amplitude of various LFP frequency bands during a three-dimensional (3-D) center-out reaching task, and found that the strongest correlation was between the arm position and the high-frequency (60-200 Hz) band.

Asher et al. (2007) also found correlation between LFPs recored in PPC and target direction, as well as object type during a prehension task. Stark and Abeles (2007) performed reach direction and grasp type decoding from LFPs from M1 and the dorsal premotor cortex (PMd), whereas Spinks et al. (2008) decoded grasp type from LFP signals in M1 and PMv.

Zhuang et al. (2010) used a Kalman filter to decode 3-D reach and grasp kinematic parameters from LFPs during free reach to grasp behaviour by using a range of LFP frequency bands, and found that the highest performance was achieved by using the high-frequency (200-400 Hz) band. The same group (Bansal et al., 2011, 2012), compared 3-D kinematics decoding during free behaviour from SA, MUA and different LFP frequency bands from M1 and PMv, and found that decoding was best when using spikes. For small numbers of input channels (1-3), however, it was shown that the high-frequency LFP band outperformed spikes. Decoding performance was increased when a hybrid-decoder was used, that is a decoder which combined both SA and LFP signals, hence suggesting that there was additional information in the LFP signals which was not included in the spike trains.

More recently, a Wiener cascade filter (Westwick et al., 2006; Pohlmeyer et al., 2007) was used to decode target location and trajectories (Flint et al., 2012b), as well as upper-limb EMG activity (Flint et al., 2012a) from LFP recordings in M1 and PMd. For EMG prediction, the high-frequency band (200-300 Hz) achieved the best decoding performance among the different LFP frequency bands examined in the study. Finally, Hwang and Andersen (2013) decoded reach target from SA and LFPs from PRR and found that single LFP channels were more informative than single spike channels, but when multiple channels were used spikes outperformed LFPs.

2.2 Feature selection for decoding movement-related information from cortical signals

In decoding paradigms of movement-related information (e.g. kinematics, muscle activity, grasp type etc.) from cortical signals (i.e. SA and LFP signals), the number of input variables is usually very large. This can turn out to be deleterious in some cases, especially when the amount of available training data is limited. In this section, we review the methods proposed in the literature for performing variable selection in order to optimise decoding performance.

Pohlmeyer et al. (2007) used 66 SA signals recorded simultaneously from M1 of monkeys to predict upper-limb muscle activity during reaching, by using a Wiener cascade filter. For selecting the optimal neural signals, a neuron dropping method was used (Westwick et al., 2006). Briefly, the unique contribution of each channel to the prediction of each output was calculated, by taking into account the information available from all the remaining channels. The unit which yielded the lowest contribution was then dropped from the pool of signals, and this process was repeated with the remaining signals. At the end of this iterative process, the input signals were chosen based on their ranks of contribution.

Ting et al. (2010) used a variational Bayesian least squares (VBLS) algorithm to predict the EMG activity of 11 muscles from 71 SA signals from M1. They compared their results to a variety of regression algorithms, including the least absolute shrinkage and selection operator (LASSO), ridge regression, stepwise regression and partial least squares (PLS), and showed that the VBLS algorithm outperformed all other methods.

Bansal et al. (2011) compared kinematics prediction from SA and LFP signals from M1 and PMv during a 3-D reaching and grasping task. For both spikes and LFPs, they used a greedy-selection procedure to identify the subset which achieved the optimal decoding performance. Briefly, the algorithm first selected the best channel or unit which individually yielded the highest decoding accuracy. At each subsequent step, the neural signal that contributed the most independent information was added to the pool of selected signals. The number of of selected inputs was restricted to a maximum of 50 signals.

A simpler approach was adopted by Flint et al. (2012a), where upper-limb muscle activity was decoded from LFP signals in M1 of primates. The total number of features in this study totalled up to 576, as six spectral features were extracted from each of the 96 simultaneously recorded LFP channels. The 150 features which were individually most

strongly correlated with the EMG signals were selected for decoding. The correlation between neural signals and EMGs was determined by the mean absolute value of the Pearson-r correlation coefficient over all muscles, and separately for each datafile.

Finally, Shin et al. (2012) decoded upper-limb muscle activity from ECoG signals in M1 of primates. For feature selection and decoding, the variational bayesian sparse regression (VBSR) algorithm (Sato, 2001) was used. Briefly, the algorithm estimates the linear weight and automatic relevance detection (ARD) parameters, which represent the relative contribution of each input to the outputs. Based on the ARD values, the method selects the relevant input variables, while at the same time sets the linear weights for the irrelevant features to zero.

2.3 Summary

LFP signals from motor cortical areas have been used to decode various movement-related parameters in primates, including upper-limb muscle activity. Nevertheless, no study so far has shown that it is possible to decode EMG activity during naturalistic free behaviour. This was the first objective of our study and, in that sense, this work can be thought as an extension to the work of Flint et al. (2012a). Additionally, a wide variety of tools have been used in the literature to perform feature selection for decoding paradigms from SA and LFP signals, but no systematic comparison of these methods has yet been performed for EMG decoding from LFPs. In the second part of our study, we systematically compared the various feature selection and regression algorithms proposed in the literature, in terms of their achieved EMG decoding accuracy.

In the following chapter, we present the surgical and experimental methods for data collection, as well as the pre-processing procedures applied to both LFP and EMG signals. Subsequently, we provide the theoretical background of the various dimensionality reduction and regression algorithms examined in this work.

Chapter 3

Methods

In this chapter, the methods used for data collection and analyses are presented. First, the surgical procedures and experimental setup are briefly described. Then, the data recording and pre-processing procedures of both EMG and cortical (spike, LFP) signals are detailed. Subsequently, the background of the different algorithms used for decoding EMG activity from cortical signals is given. Finally, a noise reduction method, as well as the discarding process for the EMG signals is presented, and a summary of the data used in this study is provided.

3.1 Surgical procedures

All procedures were carried in accordance with the UK Animals (Scientic Procedures) Act 1986 and approved by the local ethics committee of Newcastle University. One female monkey (Macaca mullata), implanted with chronic moveable tungsten microwire electrodes in M1 and PMv, as well as one floating microelectrode array (FMA)[1] implanted in M1, was used in this study. The microwire implants consisted of 12 Teflon-unsulated 50-μm-diameter tungsten wires running inside polyamide guide tubes. The FMA consisted of a 44-channel electrode array housed in 44-hole ceramic substrate with 400-μm hole separation. Full details of surgical procedures can be found in Jackson and Fetz (2007).

[1] http://www.microprobes.com/index.php/products/multi-channel-arrays/fma-floating-microelectrode-arrays

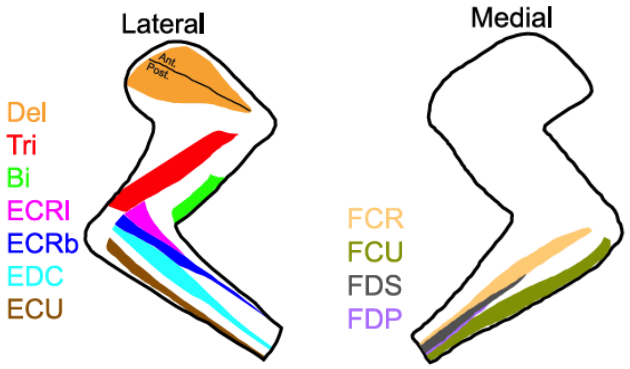

(a) (b)

Figure 3.1: Schematic of recorded limb muscle locations. Both lateral (*a*) and medial (*b*) views are shown. Adapted from Flint et al. (2012a).

3.2 Behavioural training

The subject was trained to perform a torque tracking task. At the end of each recording session, an excerpt of free behaviour was additionally recorded. During the free behaviour sessions, the subject sat in a primate chair and reached freely for small pieces of food (nuts, raisins) located in a Klüver board with its left hand. The monkey was trained to hold its right hand still for the duration of task. In the current study, only data from the free behaviour sessions were used for analyses.

3.3 Recording procedures

3.3.1 Cortical signals

Cortical signals were acquired by a digitizing pre-amplifier (sampling frequency 48.8 kHz; frequency response 3 dB for 0.35 Hz and 7.5 kHz, 6 dB for 0.2 Hz and 8.5 kHz). LFP signals were then extracted by digitally low-pass filtering the signal at 300 Hz, then downsampling to 488 Hz. Neuronal SA was extracted by digitally band-pass filtering the raw signal (1 kHz to 8 kHz), then thresholding. Single-unit spikes were classified in a semi-supervised fashion using the TDT[2] online principal component-based feature-extraction and clustering software. Spike waveforms were sampled at 24.4 kHz.

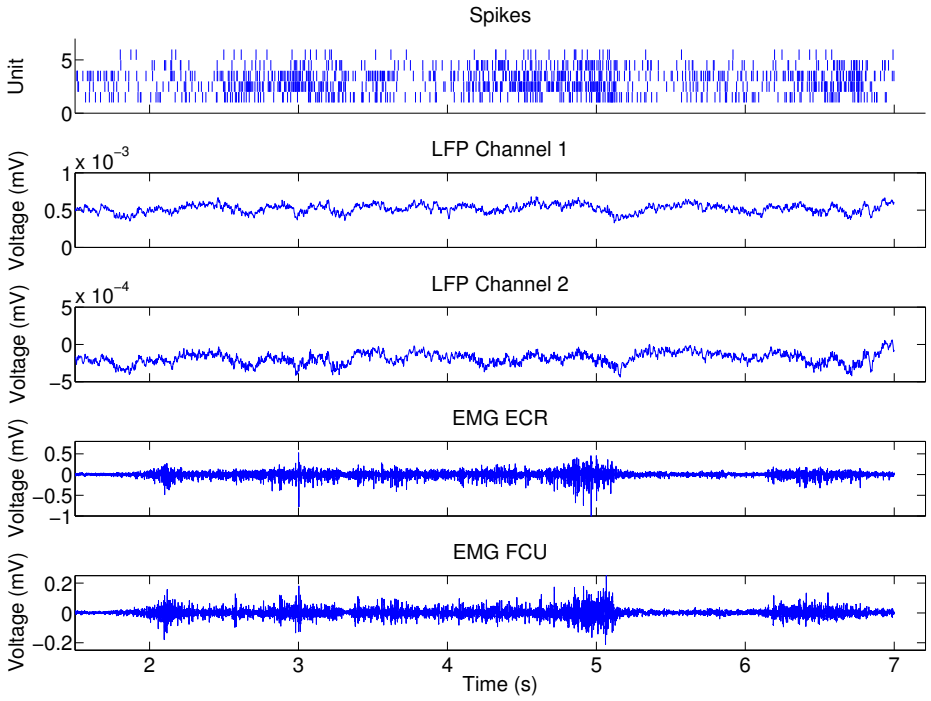

Figure 3.2: Raw data. The SA of 5 single-units is shown, along with two LFP channels and the EMG signals from ECR and FCU muscles.

3.3.2 EMG signals

EMG activity from the following 9 upper-limb muscles was recorded intramuscularly, simultaneously to cortical signals (Fig. 3.1): extensor carpi radialis (ECR), flexor carpi ulnaris (FCU), biceps (Bi), extensor carpi ulnaris (ECU), flexor carpi radialis (FCR), triceps (Tri), first dorsal interosseous (1DI), flexor digitorum superficialis (FDS), flexor digitorum profundus (FDP). EMGs were band-pass filtered from 10 Hz to 5 kHz (with a 50 Hz notch filter), and subsequently sampled at 12.2 kHz. EMG wires were routed subcutaneously to a connector that was mounted on the scalp in a head case that housed the cortical electrodes.

Fig. 3.2 shows a sample of the raw data containing the SA from 5 units in M1, two LFP channels and two EMG signals. The duration of the shown excerpt is 5.5 sec.

[2] http://www.tdt.com/software/for_neuro.htm

3.4 Data pre-processing

3.4.1 Cortical signals

The neural firing rates were determined by inverting the spike count of action potentials that fell within successive 51.2 ms bins (Pohlmeyer et al., 2007).

Following Flint et al. (2012a), six spectral features were extracted from each LFP signal: the local motor potential (LMP), which is a sliding window average of the raw LFP, and the power in five frequency bands: LF (0-4 Hz), MF1 (7-20 Hz), MF2 (70-115 Hz), HF1 (130-200 Hz) and HF2 (200-300 Hz). The power in each band was computed by applying a Hanning window and the fast fourier transform (FFT). For each time window, the log power was normalised by subtracting the log of the mean power in each band over the entire datafile. All features were computed in 256-point windows, with 231-point overlap, which provided one sample every 51.2 ms.

3.4.2 EMG signals

The EMG signals were digitally processed as follows, in order to extract their temporal envelopes: high-pass filtered at 50 Hz (4th-order Butterworth filter), full-wave rectified, low-pass filtered at 5 Hz (4th-order Butterworth filter) and, finally, downsampled at 19.5 Hz. All digital filtering was performed both forward and backward in time to avoid introducing phase delays in the output signal (Flint et al., 2012a).

3.5 Decoding

In this section, the different methods used for muscle activity decoding are presented and explained in detail. Firstly, the Wiener cascade filter (Westwick et al., 2006) is presented, which is one of the most commonly used decoding techniques in the literature (Flint et al., 2012a; Pohlmeyer et al., 2007; Ethier et al., 2012), and served as the baseline for comparison in our study. Secondly, a decoding technique based on ridge regression is described and, subsequently, a brief description of a technique based on LASSO and elastic net is given. Finally, the VBSR algorithm is presented and briefly described.

In our analyses, we tested muscle activity prediction in two different training scenarios, that is decoding with a) limited, and b) large amount of training data (Nazarpour et al., 2012). In the first case, the datafiles used were 5 minutes long, of which 3 minutes were

used for training, and the remaining 2 minutes were used for validation. In the latter case, the datafiles were 15 minutes long, of which 9 minutes were used for training and 6 minutes for validation. The reason for using such a large proportion of the available data for validation (i.e. 40%) was that, as recordings came from feely-behaving animals, we needed to ensure that the validation samples would be long enough to include non-silent epochs.

3.5.1 Wiener cascade model

A Wiener cascade model is a nonlinear model consisting of a dynamic linear subsystem followed by a static nonlinearity. In this framework, each EMG signal is treated as a multiple-input-single-output (MISO) subsystem, in which each neural input is convolved with its finite impulse response function (Westwick et al., 2006):

$$z\left(t\right) = \sum_{k=1}^{N} \sum_{\tau=0}^{M-1} h_k\left(\tau\right) x_k\left(t-\tau\right), \tag{3.1}$$

where $z\left(t\right)$ denotes the EMG activity at time t, $h_k\left(\tau\right)$ accounts for the contribution of the input k at time instance τ, $x_k\left(t-\tau\right)$ is the activation of the input k at time $t-\tau$, and we also assume a finite number of samples, i.e. $t = 1, \ldots, T$. The linear system described by Eq. 3.1 can be written in matrix form as follows:

$$\vec{z} = \mathbf{X}\vec{h} + \vec{w}, \tag{3.2}$$

where $\vec{z}$ and $\vec{w}$ are T element vectors containing $z(t)$ and $w(t)$, respectively, while $\vec{h}$ is a $N \times M$ element vector:

$$\vec{h} = \left[h_1\left(0\right) h_1\left(1\right), \ldots, h_1\left(M-1\right) h_2\left(0\right) h_2\left(1\right), \ldots, h_N\left(M-1\right)\right]^T, \tag{3.3}$$

and $\mathbf{X}$ is a block matrix

$$\mathbf{X} = \left[\mathbf{X_1}, \mathbf{X_2}, \ldots, \mathbf{X_N}\right], \tag{3.4}$$

where the $\mathbf{X_k}$ are $T \times M$ matrices

$$\mathbf{X_k} = \begin{bmatrix} x_k(1) & 0 & \ldots & 0 \\ x_k(2) & x_k(1) & \ldots & 0 \\ \vdots & \vdots & \ddots & \vdots \\ x_k(T) & x_k(T-1) & \ldots & x_k(T-M+1) \end{bmatrix}. \tag{3.5}$$

Eq. 3.2 can be solved analytically by using the normal equation:

$$\hat{\vec{h}} = \left(\mathbf{X}^T\mathbf{X}\right)^{-1}\mathbf{X}^T\vec{z}, \tag{3.6}$$

but the inversion of the matrix $\mathbf{X}^T\mathbf{X}$ can become computationally extremely expensive for large number of inputs.

An efficient solution to the MISO system identification problem can be achieved by considering the equivalent input-output relationship based on auto- and cross-correlation matrices (Perreault et al., 1999):

$$\begin{bmatrix} \vec{\phi}_{x_1 z} \\ \cdots \\ \vec{\phi}_{x_N z} \end{bmatrix} = \begin{bmatrix} \mathbf{\Phi}_{x_1 x_1} & \cdots & \mathbf{\Phi}_{x_1 x_N} \\ \vdots & \ddots & \vdots \\ \mathbf{\Phi}_{x_N x_1} & \cdots & \mathbf{\Phi}_{x_N x_N} \end{bmatrix} \begin{bmatrix} \vec{h}_1 \\ \vdots \\ \vec{h}_N \end{bmatrix}, \tag{3.7}$$

where $\vec{h}_k$ is a T element vector, $\vec{\phi}_{x_k z}$ is an M element vector containing the cross-correlation $\phi_{x_k z}(\tau)$ and $\mathbf{\Phi}_{x_k x_l}$ is an $M \times M$ Toeplitz matrix with elements $\mathbf{\Phi}_{x_k x_l}(i,j) = \phi_{x_k x_l}(i-j)$. In matrix form, Eq. 3.7 can be written as:

$$\vec{\Phi}_{Xz} = \mathbf{\Phi}_{XX}\vec{h}. \tag{3.8}$$

Hence, the solution of Eq. 3.8 is given through inversion of the the matrix $\mathbf{\Phi}_{XX}$:

$$\hat{\vec{h}} = \mathbf{\Phi}_{XX}^{-1}\vec{\Phi}_{Xz}. \tag{3.9}$$

In our implementation, the inputs x_k consisted in either neural firing rates, spectral features of LFP signals, or a combination of these two types of signals, depending on the nature of the decoder used in each case. After the linear filters were estimated using Eq. 3.7 and 3.9, the nonlinearity was introduced by fitting a third-order polynomial between the output of the linear system prediction and the recorded EMG signal of the training data.

3.5.2 Wiener-150 cascade model

The above described Wiener cascade model makes use of all the system inputs to predict the output EMG signals. However, for LFP-based decoders for which the number of input features is large (i.e. 336 features in our case), the number of fitting parameters can become extremely large (i.e. 3360 parameters when using decoders of $N = 10$ bins), which is likely to result in overfitting the training data.

One way of reducing the number of fitting parameters is by choosing the 150 features which are individually most strongly correlated with the EMG signals (Flint et al., 2012a). For this method, which will be hereafter referred to as the *Wiener-150 cascade model*, the correlation is determined by the mean of the absolute value of the Pearson correlation coefficient, r, over all muscles for each datafile.

3.5.3 Ridge regression cascade model

Now, let us consider the usual linear regression model: given p predictors $\boldsymbol{x_1}, \ldots, \boldsymbol{x_p}$, the response y is predicted by:

$$\boldsymbol{y} = \boldsymbol{X}\hat{\boldsymbol{\beta}} + \boldsymbol{\epsilon}, \tag{3.10}$$

where $y \in \mathbb{R}^n, \boldsymbol{X} \in \mathbb{R}^{n \times p}, \beta \in \mathbb{R}^p, \epsilon \in \mathbb{R}^n$ and n denotes the number of observations. The ordinary least squares (OLS) solution minimises the residual sum of squares $(\boldsymbol{y} - \boldsymbol{X}\boldsymbol{\beta})^T (\boldsymbol{y} - \boldsymbol{X}\boldsymbol{\beta})$ and is given by:

$$\hat{\boldsymbol{\beta}}_{OLS} = \left(\boldsymbol{X}^T\boldsymbol{X}\right)^{-1}\boldsymbol{X}^T\boldsymbol{y}. \tag{3.11}$$

One disadvantage of the OLS method is that the estimates often have low bias but high variance. Ridge regression (Tikhonov, 1943), is a technique which minimises the residual sum of squares subject to a bound on the L_2-norm of the coefficients, which is $(\boldsymbol{y} - \boldsymbol{X}\boldsymbol{\beta})^T (\boldsymbol{y} - \boldsymbol{X}\boldsymbol{\beta}) + \lambda\boldsymbol{\beta}^T\boldsymbol{\beta}$. The ridge regression solution is given by:

$$\hat{\boldsymbol{\beta}}_{ridge} = \left(\boldsymbol{X}^T\boldsymbol{X} + \lambda\boldsymbol{I}_n\right)^{-1}\boldsymbol{X}^T\boldsymbol{y}. \tag{3.12}$$

For $\lambda \to 0$, $\hat{\boldsymbol{\beta}}_{ridge} \to \hat{\boldsymbol{\beta}}_{OLS}$, while for $\lambda \to \infty$, $\hat{\boldsymbol{\beta}}_{ridge} \to \mathbf{0}$.

The main disadvantage of the ridge regression technique is that the parameter λ needs to be set manually. The optimal selection for this parameter can be found through cross-validation (CV) (Bishop, 2006), although the computational cost of the algorithm in this case increases dramatically. In our implementation, the λ parameter was alternated from 1 to 1000, with a constant stepsize of 10. The value that yielded the best decoding performance, as determined by the variance accounted for (VAF) measure (see Section 3.7), was selected and used for each datafile.

As with previous models, a third-order polynomial was used to fit the output of the linear prediction to the recorded EMG signals of the training data.

3.5.4 LASSO and elastic net cascade model

3.5.4.1 LASSO

The LASSO (Tibshirani, 2011), is a non-linear penalised least squares technique imposing an L_1-penalty on the regression coefficients, i.e. the LASSO solution satisfies:

$$\hat{\boldsymbol{\beta}}_{LASSO} = \arg\min \left(\boldsymbol{y} - \boldsymbol{X}\boldsymbol{\beta}\right)^T \left(\boldsymbol{y} - \boldsymbol{X}\boldsymbol{\beta}\right) + \lambda \left\|\boldsymbol{\beta}\right\|_1, \tag{3.13}$$

where $\left\|\boldsymbol{\beta}\right\|_1 = \sum_{i=1}^{p} \beta_i$ is the L_1-norm. The LASSO method solves the regression problem through an iterative algorithm, which is guaranteed to converge in a finite number of steps.

The main advantage of the LASSO technique is that some coefficients are shrinked to zero, producing hence sparse interpretable models. Similarly to ridge regression, the regularisation parameter needs to be set manually, and the optimal selection for this parameter can be found via CV. In our implementation, 100 different values of λ were tested and a 5-fold CV procedure was used to select the optimal value of the parameter.

3.5.4.2 Elastic net

The elastic net (Zou and Hastie, 2005), is a regularisation technique which combines the LASSO and ridge regression penalties, which is the L_1- and L_2-norms, respectively. The elastic net solution thus satisfies:

$$\hat{\boldsymbol{\beta}}_{elastic} = \arg\min \left(\boldsymbol{y} - \boldsymbol{X}\boldsymbol{\beta}\right)^T \left(\boldsymbol{y} - \boldsymbol{X}\boldsymbol{\beta}\right) + \lambda_2 \left\|\boldsymbol{\beta}\right\|^2 + \lambda_1 \left\|\boldsymbol{\beta}\right\|_1 . \tag{3.14}$$

The elastic penalty can take the form $J\left(\boldsymbol{\beta}\right) = \alpha \left\|\boldsymbol{\beta}\right\|^2 + (1-\alpha)\left\|\boldsymbol{\beta}\right\|_1$, where $\alpha = \frac{\lambda_2}{\lambda_2+\lambda_1}$. For $\alpha \to 0$, $\hat{\boldsymbol{\beta}}_{elastic} \to \hat{\boldsymbol{\beta}}_{LASSO}$, while for $\alpha \to 1, \hat{\boldsymbol{\beta}}_{elastic} \to \hat{\boldsymbol{\beta}}_{ridge}$.

One advantage of the elastic net technique over LASSO is that it encourages a grouping effect of the variables; correlated predictors are in or out of the model together. The main disadvantage of the method is that the optimal selection of the tuning parameters λ_1 and α requires to cross-validate over a two-dimensional surface. In our implementation, 100 different values for λ_1 and 10 different values for α (from 0.1 to 1, with 0.1 stepsize), were tested.

As for the rest of the models described above, a third-order polynomial was used to fit the output of both LASSO and elastic net predictions to the recorded EMG signals.

3.5.5 VBSR cascade model

The VBSR (Sato, 2001), is an algorithm for online model selection which defines the free energy for a trial probability distribution and approximates the joint posterior probability distribution over model parameters and hidden variables. The maximisation of the free energy gives the true posterior distribution over the parameters and hidden variables. The integration over model parameters is done with an expectation-maximisation (EM) algorithm.

Let us consider a set of models $\{\mathcal{M}_m | m = 1, \ldots, \mathcal{N}\}$, where $\mathcal{M}_m$ denotes a model with fixed structure. Let $P\left(\boldsymbol{x}|\boldsymbol{\theta}_m, \mathcal{M}_m\right)$ denote the probability distribution of a model $\mathcal{M}_m$ with parameter $\boldsymbol{\theta}_m$, where $\boldsymbol{x}$ represents a random variable and $\boldsymbol{X}\left\{T\right\} = \left\{\boldsymbol{x}\left(t\right) | t = 1, \ldots, T\right\}$

is a set of observed data. The posterior probability over the parameter is given by Bayes rule:

$$P\left(\boldsymbol{x}|\boldsymbol{\theta}_m, \mathcal{M}_m\right) = \frac{P\left(\boldsymbol{X}\left\{T\right\}|\boldsymbol{\theta}_m, \mathcal{M}_m\right) P\left(\boldsymbol{\theta}_M|\mathcal{M}_m\right)}{P\left(\boldsymbol{X}\left\{T\right\}|\mathcal{M}_m\right)}. \tag{3.15}$$

The data likelihood is defined by

$$P\left(\boldsymbol{X}\left\{T\right\}|\boldsymbol{\theta}_m, \mathcal{M}_m\right) = \prod_{t=1}^{T} P\left(\boldsymbol{x}\left\{T\right\}|\boldsymbol{\theta}_m, \mathcal{M}_m\right), \tag{3.16}$$

where $\mathcal{M}_m$ denotes the evidence for a model, defined by

$$P\left(\boldsymbol{X}\left\{T\right\}|\mathcal{M}_m\right) = \int d\mu\left(\boldsymbol{\theta}_m\right) P\left(\boldsymbol{X}\left\{T\right\}|\boldsymbol{\theta}_m, \mathcal{M}_m\right) P\left(\boldsymbol{\theta}_M|\mathcal{M}_m\right), \tag{3.17}$$

and the posterior probability distribution over model structure is given by

$$P\left(\mathcal{M}_m|\boldsymbol{X}\left\{T\right\}\right) = \frac{P\left(\boldsymbol{X}\left\{T\right\}|\mathcal{M}_m\right) P\left(\mathcal{M}_m\right)}{\sum\limits_{m'} P\left(\boldsymbol{X}\left\{T\right\}|\mathcal{M}_{m'}\right) P\left(\mathcal{M}_{m'}\right)}. \tag{3.18}$$

The evidence for a data set $\boldsymbol{X}\left\{T\right\}$ is defined by:

$$P\left(\boldsymbol{X}\left\{T\right\}\right) = \int d\mu P\left(\boldsymbol{X}\left\{T\right\}|\boldsymbol{\theta}\right) P_0\left(\boldsymbol{\theta}\right), \tag{3.19}$$

where $P_0\left(\boldsymbol{\theta}\right)$ denotes a prior distribution for the model parameters. In order to perform the integration, the variational bayes (VB) method uses a trial probability distribution $Q\left(\boldsymbol{\theta}, \boldsymbol{Z}\left\{T\right\}\right)$, which approximates the posterior distribution over the model parameter $\boldsymbol{\theta}$, where $\boldsymbol{Z}\left\{T\right\}$ denotes a set of hidden variables $\boldsymbol{Z}\left\{T\right\} = \left\{\boldsymbol{z}\left(t\right)|t = 1, \ldots, T\right\}$ and $\boldsymbol{z} = \left(z_1, \ldots, z_M\right)^T$:

$$P\left(\boldsymbol{\theta}, \boldsymbol{Z}\left\{T\right\}|\boldsymbol{X}\left\{T\right\}\right) = \frac{P\left(\boldsymbol{X}\left\{T\right\}, \boldsymbol{Z}\left\{T\right\}|\boldsymbol{\theta}\right) P_0\left(\boldsymbol{\theta}\right)}{P\left(\boldsymbol{X}\left\{T\right\}\right)}, \tag{3.20}$$

where the probability distribution for a complete dataset is given by

$$P\left(\boldsymbol{X}\left\{T\right\}, \boldsymbol{Z}\left\{T\right\}|\boldsymbol{\theta}\right) = \prod_{t=1}^{T} P\left(\boldsymbol{x}\left\{T\right\}, \boldsymbol{z}\left\{T\right\}|\boldsymbol{\theta}\right). \tag{3.21}$$

According to the Kullback-Leibler (KL) divergence between the trial and the true posterior distribution:

$$\begin{aligned} KL\left(Q||P\right) &= \int d\mu\left(\boldsymbol{\theta}\right) d\mu\left(\boldsymbol{Z}\left\{T\right\}\right) Q\left(\boldsymbol{\theta}, \boldsymbol{Z}\left\{T\right\}\right) \times \log\left(\frac{Q\left(\boldsymbol{\theta}, \boldsymbol{Z}\left\{T\right\}\right)}{P\left(\boldsymbol{\theta}, \boldsymbol{Z}\left\{T\right\}|\boldsymbol{X}\left\{T\right\}\right)}\right) \\ &= \log P\left(\boldsymbol{X}\left\{T\right\}\right) - F\left(\boldsymbol{X}\left\{T\right\}, Q\right), \end{aligned} \tag{3.22}$$

where the *free energy* is defined by

$$F\left(\boldsymbol{X}\left\{T\right\}, Q\right) = \int d\mu\left(\boldsymbol{\theta}\right) d\mu\left(\boldsymbol{Z}\left\{T\right\}\right) Q\left(\boldsymbol{\theta}, \boldsymbol{Z}\left\{T\right\}\right) \times \log\left(\frac{P\left(\boldsymbol{X}\left\{T\right\}, \boldsymbol{Z}\left\{T\right\}|\boldsymbol{\theta}\right) P_0\left(\boldsymbol{\theta}\right)}{Q\left(\boldsymbol{\theta}, \boldsymbol{Z}\left\{T\right\}\right)}\right). \tag{3.23}$$

The true posterior distribution is obtained by maximising the free energy with respect to the trial distribution $Q(\boldsymbol{\theta}, \boldsymbol{Z}\{T\})$, and this maximum of the free energy is equal to the log evidence:

$$\log P(\boldsymbol{X}\{T\}) = \max_{Q} F(\boldsymbol{X}\{T\}, Q) \geq F(\boldsymbol{X}\{T\}, Q). \tag{3.24}$$

For the purposes of implementation, the VBSR toolbox[3] for MATLAB® was used. Similarly to previously described algorithms, a third-order polynomial was used to fit the output of the prediction and the recorded EMG signals of the training data.

3.6 Filter size

The filter size (or kernel size), i.e. the number of bins used for decoding, for all the above described methods was set to $N = 10$ bins, unless where stated otherwise. This translates to a time course of $51.2 \times 10 = 512$ ms.

3.7 Performance assessment

As a measure of performance of the EMG prediction from cortical signals, two different measures were used: the variance accounted for (VAF), and the coefficient of determination (R^2). These are defined as follows:

$$VAF = 1 - \frac{\sum_{j=1}^{M} (p_j - \hat{p}_j)^2}{\sum_{j=1}^{M} (p_j - \bar{p})^2}, \tag{3.25}$$

and

$$R^2 = \frac{\left(\sum_{j=1}^{M} (p_j - \bar{p})(\hat{p}_j - \bar{\hat{p}}) \right)^2}{\sum_{j=1}^{M} (p_j - \bar{p})^2 \sum_{j=1}^{M} (\hat{p}_j - \bar{\hat{p}})^2}, \tag{3.26}$$

where M is the number of samples of a dataset, p_j and $\hat{p}_j$ are the actual and predicted values of the EMG signal for the j^{th} sample, and $\bar{p}$ and $\bar{\hat{p}}$ denote the mean values of the actual and predicted signals within the dataset, respectively. Although these two measures are similar, their major difference is that VAF reaches unity only with an exact match between the observed and predicted signal, compared to R^2 which

[3] http://www.cns.atr.jp/cbi/sparse_estimation/sato/VBSR.html

Datafile filename	Length (min)	SA units	EMG channels								
			ECR	FCU	Bic	ECU	FCR	Tri	1DI	FDS	FDP
Block-57	15.2508	45	+	+	+	+	+	+	+	+	+
Block-72	5.7839	56	+	+	-	+	-	-	-	+	+
Block-241	16.0098	56	+	+	-	+	+	+	+	+	+
Block-257	16.0657	56	+	+	-	+	+	-	+	+	+
Block-259	15.4820	34	+	+	-	+	-	+	+	+	+
Block-265	36.2769	56	+	+	-	+	+	+	+	+	+

Table 3.1: Summary of data used for analyses. All datafiles also included 56-channel LFP recordings.

reaches unity when the two signals are connected through a perfect linear correlation. Another difference is that for poor fits VAF can take negative values, whereas R^2 is a non-negative measure (Oby et al., 2013).

3.8 EMG de-noising and discarding process

3.8.1 Hard threshold noise reduction

In our recordings, there was noise interference in certain EMG channels. A hard threshold method was used to reduce the noise. Some other options were also considered, such as frequency-domain filtering, or independent component analysis (ICA) decomposition and reconstruction, but both were proven unsuccessful. The hard threshold θ_{thr} was chosen manually for each EMG channel and each datafile. The non-linear function used was defined by:

$$z(t) = \begin{cases} z(t), & \text{if } \|z(t)\| < \theta_{thr} \\ 0, & \text{otherwise} \end{cases}, \tag{3.27}$$

where $z(t)$ denotes EMG activity at time t.

3.8.2 Discarding process

EMG channels for which prediction accuracy from SA signals with the Wiener-150 cascade model yielded a VAF value smaller than 0.3 were treated as noisy, and were discarded from subsequent analyses. A summary of the data used for analyses is given in Table 3.1.

Chapter 4

Results

In this chapter, the results from our analyses are presented. Firstly, the Wiener-150 cascade model is tested, and the effect of tuning various model parameters on the prediction accuracy is explored. The analysis is then repeated by using M1 and PMv signals separately, and the prediction accuracy of the two different decoders is compared. The relative information about muscle activity in different LFP bands is also investigated.

Subsequently, the different decoding methods described in Chapter 3 are tested, and compared to each other in terms of prediction accuracy. The comparison of the decoding algorithms is done separately for the scenarios of large and limited amounts of training data (see Section 3.5).

4.1 Wiener-150 cascade model

Initially, we studied the accuracy of EMG prediction from LFP signals with the Wiener-150 cascade model (Flint et al., 2012a). A sample prediction of the EMG signals for datafile 'Block-57' is shown in Fig. 4.1. The overall mean prediction accuracy for the whole datafile was VAF $= 0.51 \pm 0.11$ (mean $\pm$ s.d.).

The mean accuracy prediction for all datafiles is shown in Fig. 4.2(a). Two different cases were examined; training with large amount of data (9 minutes), and training with limited amount of data (3 minutes). Additionally, three types of decoders were used; spike-, LFP- and hybrid decoders.

For long training datafiles, the results were comparable for all three types of decoders (overall mean VAF $= 0.58 \pm 0.11$ for spikes; 0.58 ± 0.11 for LFPs; 0.60 ± 0.10 for

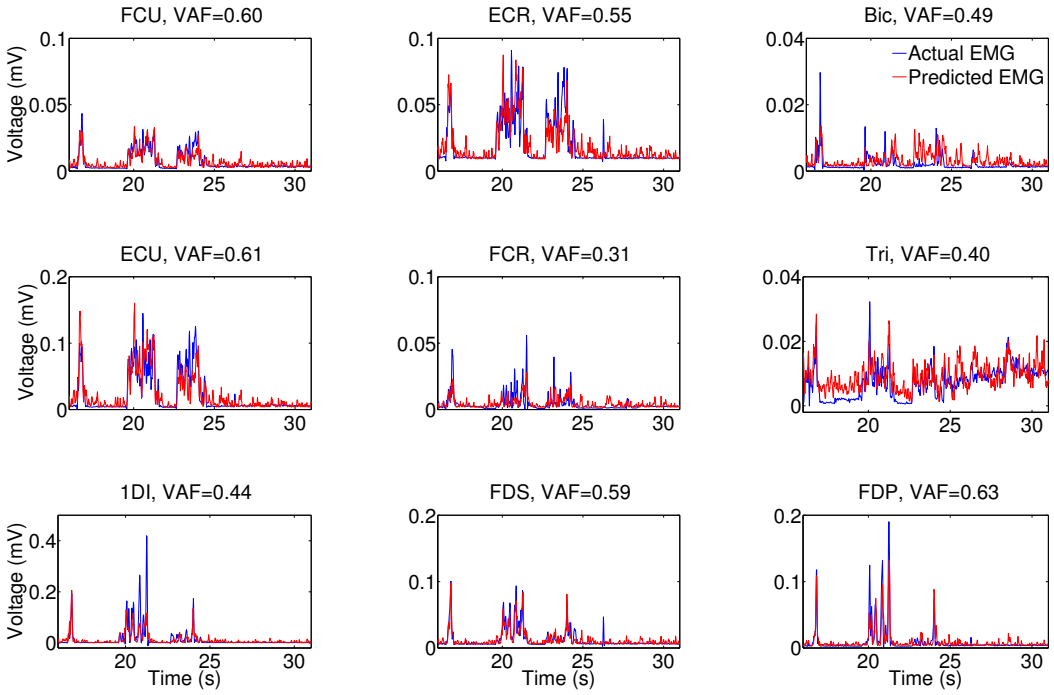

Figure 4.1: Example EMG predictions with Wiener-150 cascade model for datafile 'Block-57'.

hybrid decoders; $P > 0.3$ in all cases, paired t-tests). For short training datafiles, the spike-decoder performed significantly better than the other two (overall mean VAF = 0.45 ± 0.21 for spikes; 0.24 ± 0.28 for LFPs; 0.13 ± 0.60 for hybrid decoders, $P < 0.05$ in both cases, paired t-tests). Decoding performance for individual muscles is shown in Appendix A (Fig. A.2; results for long training datasets are only shown).

In order to evaluate whether our model yielded better predictions than chance, we randomised the rows of the coefficient matrix and measured the prediction accuracy. This procedure was repeated 100 times and the case which yielded the highest performance was selected and compared to the performance of the model. The results are shown in Fig. 4.2(b). For purposes of demonstration, the R^2 measure is shown, as the VAF took very large negative values for chance prediction. The Wiener-150 cascade model predicted better than chance for all three types of decoders (overall mean $R^2 = 0.60 \pm 0.10$ vs. 0.30 ± 0.10, $P < 10^{-20}$ for spikes; 0.59 ± 0.11 vs. 0.15 ± 0.06, $P < 10^{-35}$ for LFPs; 0.62 ± 0.10 vs. 0.22 ± 0.08, $P < 10^{-30}$ for hybrid decoders, paired t-tests).

We also tested the decoding performance of the algorithm, for EMG low-pass cutoff frequency of 10 Hz (see Section 3.4.2). The results are shown in Appendix A (Fig. A.1). As expected, the EMG prediction accuracy was slightly inferior compared to the case of 5 Hz, as in the former case the EMG signals contained more information.

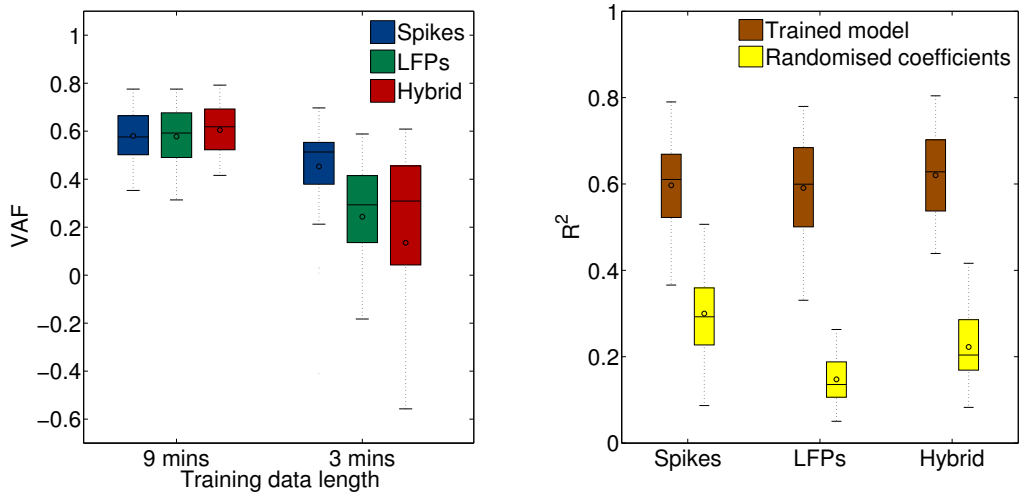

(a) (b)

Figure 4.2: EMG decoding performance with Wiener-150 cascade model. (*a*) EMG prediction accuracy for different types of decoders, and for short and long training datafiles. (*b*) Comparison of Wiener-150 cascade model performance to chance prediction. Black lines, medians; black circles, means; solid boxes, interquartile ranges; whiskers, overall ranges of nonoutlier data; data averaged across muscles and datafiles.

4.1.1 Kernel size and optimal bin for decoding

Next, we computed the EMG prediction accuracy for various sizes of kernels (Fig. 4.3(a)). For both spike- and LFP-decoders, the decoding performance reached a plateau for $N = 5$ bins. However, for the rest of analyses we selected $N = 10$ bins, in order to be consistent with previous studies (Flint et al., 2012a).

We also sought to identify the optimal lag for decoding EMG activity, when a single time bin was used for decoding (Fig. 4.3(b)). The optimal lags for decoding with spikes were 25.6 ms (the centre of the 0- to 51.2- ms bin) and 76.8 ms (the centre of the 51.2- to 102.4 ms bin), as differences between these two time lags were not significant ($P = 0.87$; paired t-test). For LFPs, the optimal time lag was 128 ms (i.e. the center of the 0- to 256- ms FFT window). For single-bin decoding, and when using the optimal lag for each type of decoder, LFP-decoders performed significantly better than spikes (overall mean VAF $= 0.49 \pm 0.11$ for spikes vs. 0.58 ± 0.11 for LFPs; $P < 10^{-3}$, paired t-test).

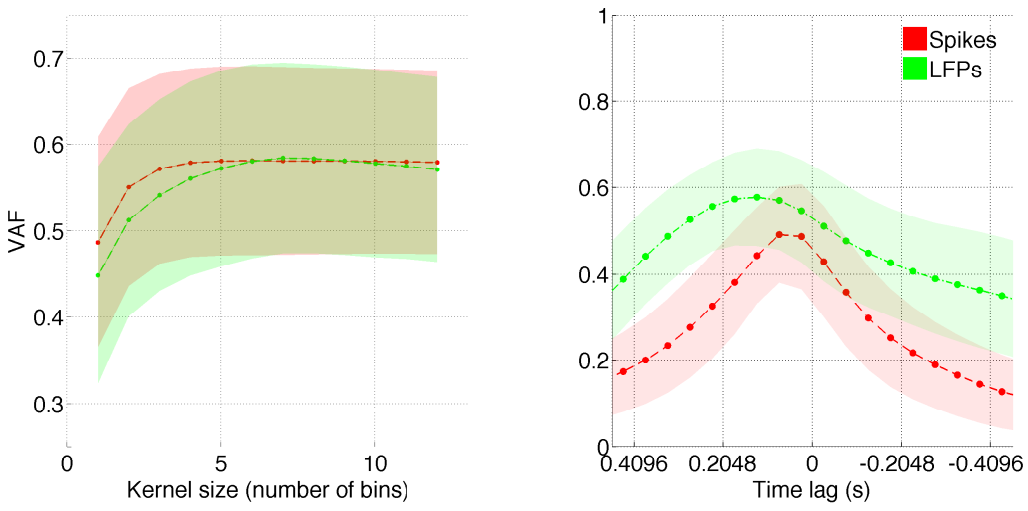

(a) (b)

Figure 4.3: Kernel size and optimal lag for decoding with Wiener-150 cascade model. (*a*) Decoding performance versus kernel size (number of bins) for decoding with spikes and LFPs. (*b*) Decoding performance using single time lags. Note reversed time axis; positive lags represent neural signals occurring before EMG activity. Thick lines, means; shaded areas, standard deviations; data averaged across muscles and datafiles.

4.1.2 M1 versus PMv decoding

In the following step, we compared the EMG prediction accuracy from M1 and PMv signals (Fig. 4.4). For M1, only recordings from the 12 microwire channels were used (see Section 3.1). Additionally, electrodes which did not record spikes where removed from the LFP-decoders, which eventually gave a number of 8.33 ± 1.5 and 5.83 ± 0.98 electrodes for M1 and PMv, respectively. The analysis was repeated without the last step (i.e. removing the additional LFP channels), and the results are shown in Appendix A (Fig. A.3). Results for individual muscles are also shown in Fig. A.4.

In general, M1-decoders yielded better performance than PMv-decoders (Fig. 4.4(b); overall mean VAF $= 0.45 \pm 0.10$ vs. 0.28 ± 0.11, $P < 10^{-5}$ for spikes; 0.53 ± 0.10 vs 0.44 ± 0.09, $P < 10^{-3}$ for LFPs; 0.60 ± 0.09 vs. 0.47 ± 0.09, $P < 10^{-5}$ for hybrid decoders, paired t-tests).

For M1 signals, the hybrid decoder performed best (Fig. 4.4(a); $P < 10^{-5}$ for spikes; $P < 0.05$ for LFPs), while the LFP- performed better than spike-decoder ($P < 10^{-2}$). For PMv, the hybrid decoder did not outperform the LFP-decoder ($P = 0.15$), but both performed better than the spike-decoder ($P < 10^{-6}$ and $P < 10^{-8}$, respectively).

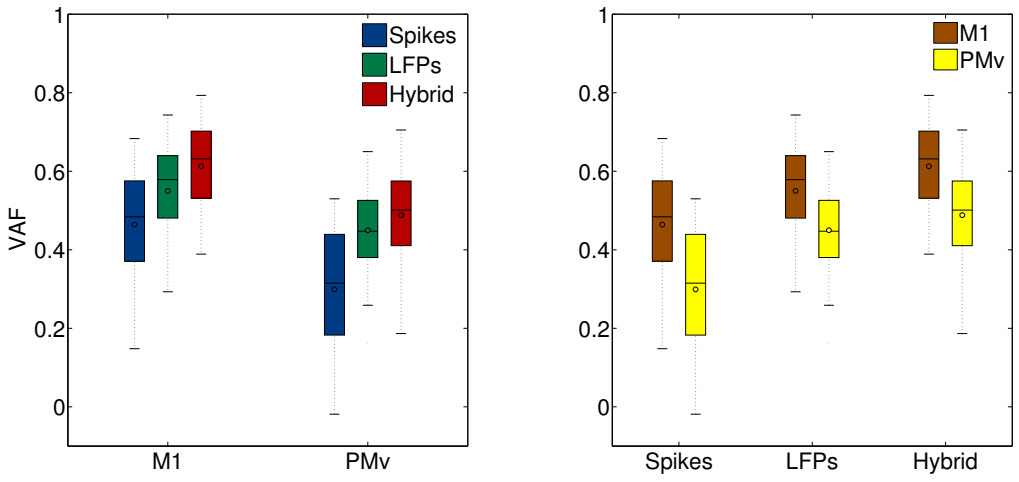

(a) (b)

Figure 4.4: M1 vs. PMv decoding with Wiener-150 cascade model. (*a*) Performance comparison for different types of decoders in M1 and PMv, separately. (*b*) Performance comparison for same type of decoders between M1 and PMv. Same number of spike and LFP channels was used. Results for long training datafiles are only shown. Data averaged across muscles and datafiles. Box symbols the same as in Fig. 4.2.

4.1.3 Remarks

We have shown that EMG prediction from SA and LFP signals in the M1 and PMv is feasible during naturalistic free behaviour by using a Wiener-150 cascade model (Fig. 4.1, 4.2). The accuracy of prediction improves with an increase in the availability of training data (Fig. 4.2(a)). For long enough training datafiles, there were no significant differences observed between the performance of spike-, LFP- and hybrid decoders, which suggests that LFPs can provide a highly informative source signal for BMIs.

Similarly to the findings of Flint et al. (2012a), the optimal lag for decoding with spikes was 25.6 ms (or 76.8 ms). For LFP-decoders, however, the same study showed that the optimal time lag was 2 ms, whereas we found that the optimal lag was 128 ms. One possible explanation for this disagreement might lie in the nature of the behavioural task, as in the above mentioned study the subjects exhibited repetitive reaching tasks, whereas in our study the animals behaved freely in their environment.

We then examined whether there were differences in prediction accuracy when we used signals only from M1 or PMv. We found that M1 signals yielded significantly better predictions for all three types of decoders (Fig. 4.4(a)). This is not in accordance with

the findings of Bansal et al. (2012), where it was shown that decoding performance from signals from M1 was comparable to the one from PMv. This disagreement might be due to differences in the behavioural tasks, as well as the nature of the prediction itself (kinematic parameters instead of muscle activity). Moreover, in our study, the number of electrodes used from each region was relatively small and, also, the number of electrodes from M1 was larger than the one from PMv (8.33 ± 1.5 electrodes for M1 vs. 5.83 ± 0.98 for PMv), making it thus difficult to draw any conclusions. We plan to verify our observations in the near future, by analysing data from additional animals.

Notably, we found that when we used only signals from PMv to make predictions, LFP signals outperformed SA signals (Fig. 4.4(b)), and this trend was systematic across muscles (Fig. A.4). To the best of our knowledge, this finding has not been reported elsewhere in the literature, although this is likely to be due to the small number of channels used for decoding in this case. It has been shown in other studies (Bansal et al., 2012; Flint et al., 2012a,b), that for small number of inputs, LFP- decoding can outperform SA- decoding. In simple terms, this can be explained by the fact that when we record the SA of a small number of cells, the chances that these cells contain information relevant to the decoded signal (e.g. kinematic parameters or EMG activity), are small. On the contrary, if we think of LFP signals as the superposition of the SA of many individual units, it is likely that even a small number of LFP signals contain some information about the decoded signal (Bansal et al., 2012).

4.2 Wiener cascade model

At this stage, we tested the decoding performance of a Wiener cascade model, which is similar as the model described in the previous section, except that all LFP features were used for decoding, i.e. the selection step of the 150 mostly correlated features to the EMG signals was omitted in this case (see Section 3.5.1). The results for long and short training datasets are shown in Fig. 4.5. For purposes of demonstration, the R^2 measure is shown, as VAF took large negative values for decoding with LFP- and hybrid decoders, in the case of short training datafiles.

For long training datafiles, spikes yielded slightly better prediction than both LFP- and hybrid decoders (overall mean VAF $= 0.58 \pm 0.11$ vs. 0.50 ± 0.11 $P < 10^{-2}$ for LFPs; 0.52 ± 0.11 $P < 0.05$ for hybrid decoders; paired-t tests). LFP- and hybrid decoders did not yield significantly different results ($P = 0.31$).

For short training datafiles, LFP- and hybrid decoders failed dramatically to predict EMG activity, most likely due to overfitting the training data, as the number of fitted

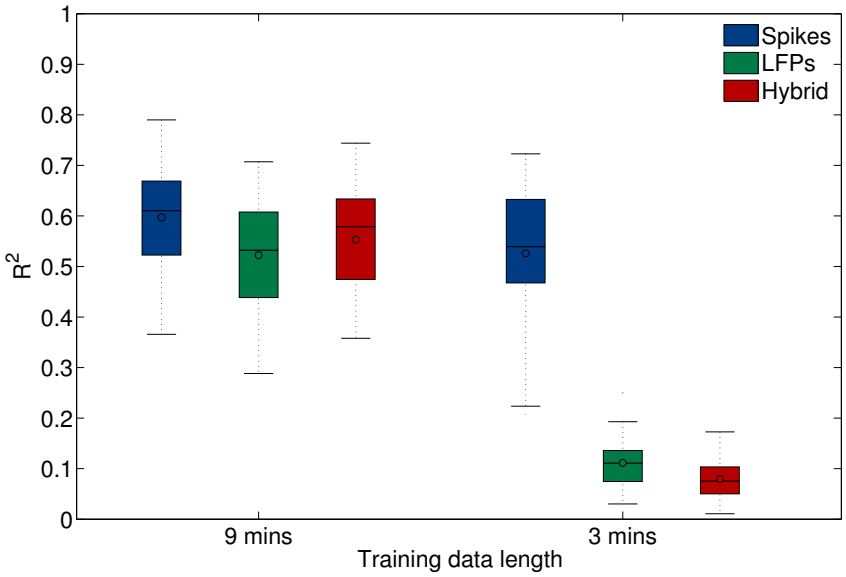

Figure 4.5: Decoding performance of Wiener cascade model, for long and short training datafiles. Box symbols the same as in Fig. 4.2.

model parameters was large (336 features $\times$10 bins = 3360 parameters), and the amount of available training data was limited ($\approx$ 4000 samples). On the other hand, spike decoders were robust, as the number of fitted model parameters was significantly smaller (56 spike channels $\times$10 bins = 560 parameters). Spikes outperformed both LFP- and hybrid decoders (overall mean VAF = 0.45 ± 0.20 vs. -8.53 ± 14.98 $P < 10^{-3}$ for LFPs; -22.36 ± 59.99 $P < 10^{-3}$ for hybrid decoders; paired-t tests). There was no significant difference between LFP- and hybrid decoders ($P = 0.14$).

4.2.1 Relative information in LFP frequency bands

The relative muscle activity information in different LFP frequency bands was investigated at this stage. For this reason, we built decoders based on separate frequency bands, or the LMP (see Section 3.4.1), and compared the performance between these decoders. The results are shown in Fig. 4.6 and Table 4.1 (results for individual muscles are given in B.1).

In general, high (130-244 Hz) and mid-high (70-115 Hz) frequency bands performed best and the performance of these decoders was comparable to the performance of the decoder using features from all frequency bands (Table 4.1).

For limited amount of training data, a decoder trained on all features failed to generalise to test datasets, although decoders trained on single frequency bands performed

Decoder source signal	VAF
LMP + all frequency bands	0.50 ± 0.11 (***LMP, LF, MF1), (†MF2, HF1, HF2)
LMP	0.37 ± 0.15 (***MF1), (†LF)
LF (0-4 Hz)	0.34 ± 0.10 (***MF1)
MF1 (7-20 Hz)	0.23 ± 0.08
MF2 (70-115 Hz)	0.47 ± 0.16 (**LMP), (***LF, MF1)
HF1 (130-200)	$\mathbf{0.54 \pm 0.12}$ (***LMP, LF, MF1), (*MF2) (†HF2)
HF2 (200-244)	0.53 ± 0.12 (***LMP, LF, MF1), (*MF2)

Table 4.1: Single-frequency band decoding performance with Wiener cascade model. Results are shown only for long training datasets. Values are means ± S.D.; $^{*}P < 0.05$; $^{**}P < 10^{-2}$; $^{***}P < 10^{-3}$; †not significant ($P > 0.05$).

relatively well (Fig. 4.6). This further supports our assumption that a decoder trained on all LFP features suffers from overfitting, unless the amount of available training data is very large.

4.2.2 Remarks

In this section, we have shown that a Wiener cascade model without feature selection can be robust in predicting muscle activity, only when a large amount of training data is available (Fig. 4.2(a)). In any other case, a feature selection process is needed to avoid overfitting the training data.

We also tested the relative muscle activity information in different frequency bands, and found that the most informative were the high-frequency bands HF2 (200-244 Hz) and H1 (130-200 Hz), followed by the mid-high band MF2 (70-115 Hz), the LMP and the low-frequency band LF (0-4 Hz). The least informative signal was the mid-low band MF1 (7-20 Hz), yet with decoding performance well above chance. This trend was almost consistent across muscles (Fig. B.1). These findings are consistent with previous studies which showed that the high frequency bands were the most robust LFP signals for reconstructing kinematic parameters (Bansal et al., 2012; Zhuang et al., 2010), or EMG activity (Flint et al., 2012a). One major difference was that EMG reconstruction from the LMP signal was of inferior quality in our study, compared to Flint et al. (2012a).

Previous studies (Logothetis, 2002; Ray et al., 2008) have suggested that high-frequency (> 200 Hz) LFP activity might reflect MUA, which is SA of a collection of individual units. It has been also speculated that these signals might also contain other fast

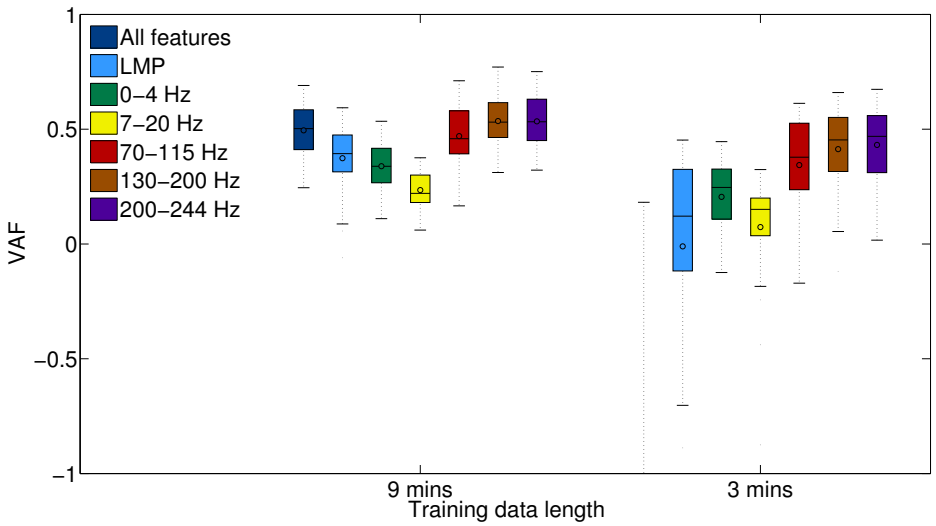

Figure 4.6: Single-frequency band decoding performance with Wiener cascade model. Results are shown for long and short training datafiles. For short training datafiles, the performance of the 'All features' decoder was VAF $= -3.6638 \pm 3.0424$ (not shown). Data averaged across muscles and datafiles. Box symbols the same as in Fig. 4.2.

synaptic components (Bansal et al., 2012). Nevertheless, our results showed that the HF1 band (130-200 Hz) allowed for equally accurate predictions as the HF2 band (200-244 Hz), whereas predictions based on the MF2 band (70-115 Hz) were slightly worse. These two latter bands (HF1 and MF2), are less likely to contain MUA activity, hence it is reasonable to speculate that they indeed convey information about movement, which is independent of SA.

4.3 Dimensionality reduction for EMG prediction from cortical signals

In the previous section, we showed that muscle activity prediction from LFP signals is feasible during naturalistic free behaviour. Nevertheless, the poor performance of the model for limited amounts of training data (Fig. 4.5), shows clearly that an effective algorithm of performing dimensionality reduction in the input of the system to be identified is essential, in order to avoid overfitting the training data. The feature selection method proposed by Flint et al. (2012a) which is based on the correlations between LFP signals and EMG activity, seems to overcome this issue (Fig. 4.2), however the selection of exactly 150 features seems somewhat arbitrary. In this section, we test the different dimensionality reduction and variable selection methods presented

Training data length	Regression method	VAF (spikes)	VAF (LFPs)	VAF (hybrid)
9 mins	Wiener	0.58 ± 0.11	0.50 ± 0.11	0.52 ± 0.11
	Wiener-150	0.58 ± 0.11	0.58 ± 0.11	0.60 ± 0.10
	LASSO/elastic net	$\mathbf{0.59 \pm 0.11}$	0.58 ± 0.11	0.61 ± 0.10
	Ridge regression	0.56 ± 0.11	0.43 ± 0.15	0.49 ± 0.16
	VBSR	0.58 ± 0.11	$\mathbf{0.61 \pm 0.11}$	$\mathbf{0.63 \pm 0.10}$
3 mins	Wiener	0.45 ± 0.20	-8.53 ± 14.98	-22.36 ± 59.99
	Wiener-150	0.45 ± 0.21	0.24 ± 0.28	0.13 ± 0.60
	LASSO/elastic net	0.42 ± 0.50	0.35 ± 0.18	0.30 ± 0.25
	Ridge regression	$\mathbf{0.51 \pm 0.14}$	0.24 ± 0.31	0.43 ± 0.18
	VBSR	0.34 ± 0.74	$\mathbf{0.53 \pm 0.17}$	$\mathbf{0.56 \pm 0.14}$

Table 4.2: Decoding performance of regression methods. Values are means ± S.D. Data averaged across muscles and datasets.

in Chapter 3, and compare their decoding performance, yet for two different training scenarios, which is for large and limited amounts of training data.

4.3.1 Decoding performance of dimensionality reduction and variable selection methods

The decoding performance of the various dimensionality reduction and variable selection techniques examined in this study is presented in Table 4.2 and Fig. 4.7.

The LASSO and elastic net algorithms yielded almost identical results (Fig. C.1), and hence, they will be hereafter treated as one algorithm and referred to as LASSO/Elastic net.

When the models were trained on 9 minutes of data, the results between the different methods were comparable, and none of the algorithms outperformed the Wiener-150 cascade model, for any type of decoder (Fig. 4.7(a)).

On the other hand, when the models were trained on 3 minutes of data, the VBSR algorithm outperformed all the other methods for LFP- and hybrid decoders, whereas for spike decoders there were not significant differences observed between the different algorithms (Fig. 4.7(b)). For LFP- and hybrid decoders, the VBSR algorithm yielded significantly better predictions than the Wiener-150 cascade model ($P < 10^{-7}$ and $P < 10^{-4}$, respectively, paired t-tests).

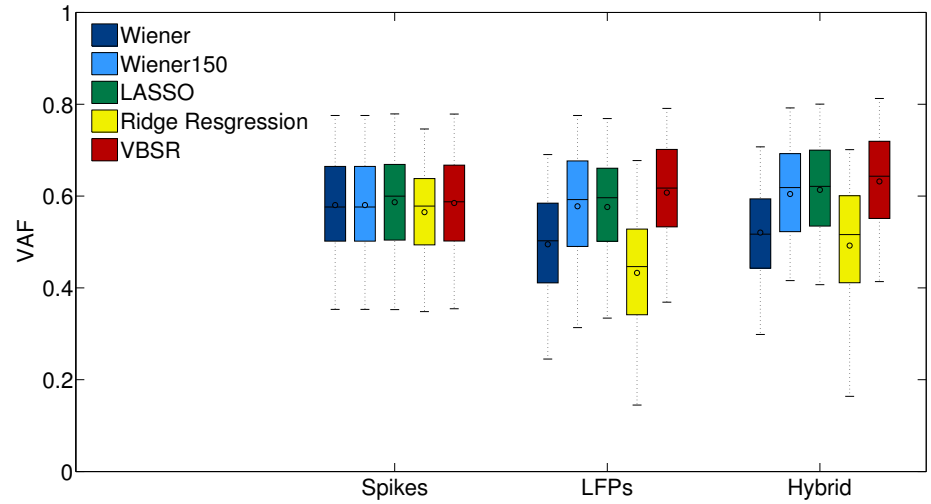

(a)

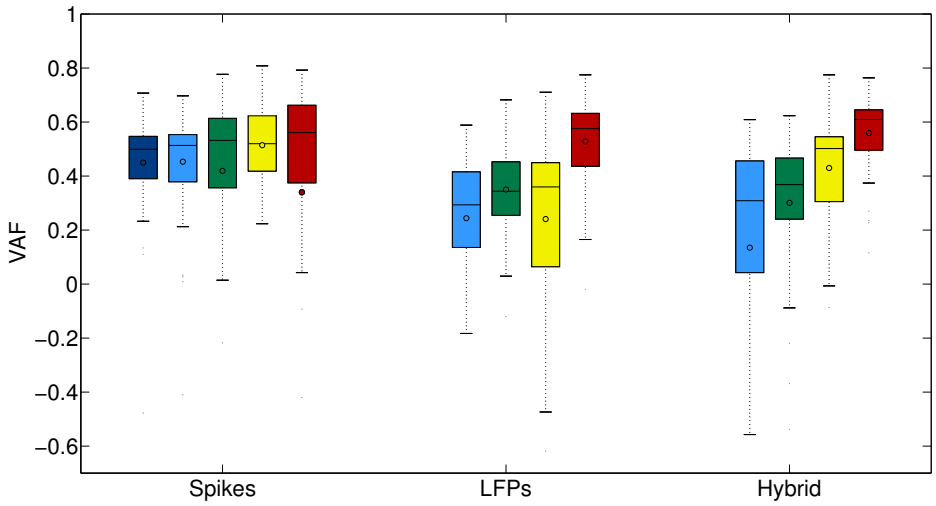

(b)

Figure 4.7: Decoding performance of regression methods for 9 mins (a) and 3 mins (b) of training data. Data averaged across muscles and datasets. Box symbols the same as in Fig. 4.2.

In Fig. 4.8 we plot the performance of LFP-decoders produced by the VBSR and Wiener-150 cascade models, versus the length of the data used for training. For purposes of demonstration, the R^2 measured is shown, as the VAF took large negative values for decoding with the Wiener-150 cascade model, when the training datafiles were shorter than 3 minutes. It can be observed, that we were able to achieve relatively accurate predictions with the VBSR cascade model, even when we used only

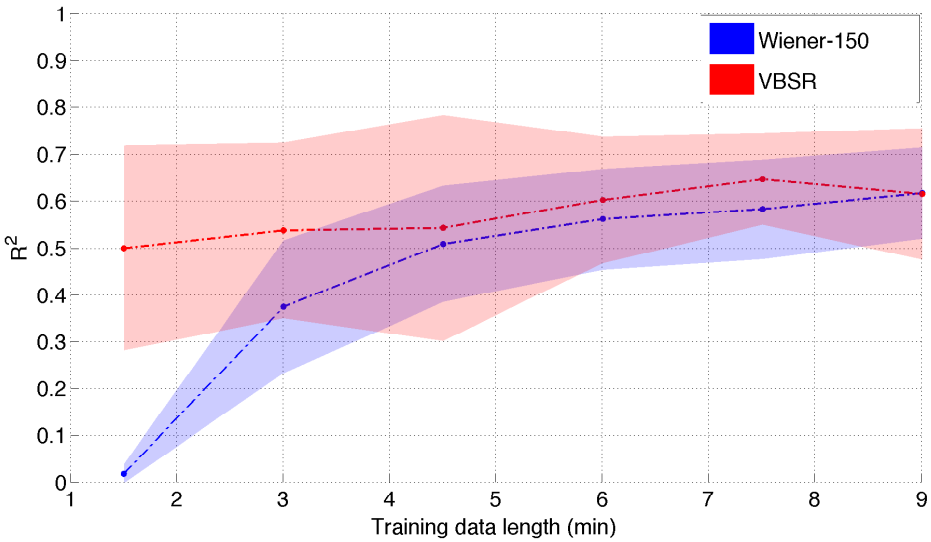

Figure 4.8: Wiener-150 and VBSR cascade models decoding performance versus training datafile length. Thick lines, means; shaded areas, standard deviations; data averaged across muscles and datafiles

1.5 minutes of training data (overall mean $R^2 = 0.50 \pm 0.22$). For training datafiles of length of 4.5 minutes and longer, the differences in performance between the two algorithms were not significant.

In order to visualise the prediction improvement with the VBSR algorithm over the Wiener-150 cascade model, we plot in Fig. 4.9 a prediction sample with each of these two algorithms, for the same time course of activity of the FCR muscle. This example clearly demonstrates that the VBSR algorithm produces more robust and less noisy predictions than the Wiener-150 cascade model.

For LFP-decoders, the average number of features selected by each method, as well

Method	Number of non-zero parameters	Execution time (s)
Wiener-150	1500 ± 0	3
LASSO/elastic net	1787 ± 733	3224
Ridge regression	3360 ± 0	3122
VBSR	1060 ± 152	622

Table 4.3: Number of selected parameters and computational time required for training regression models. For numbers of parameters, values are means ± S.D. Data averaged across muscles and datasets. For training times, each algorithm was tested once on the datafile 'Block-72'.

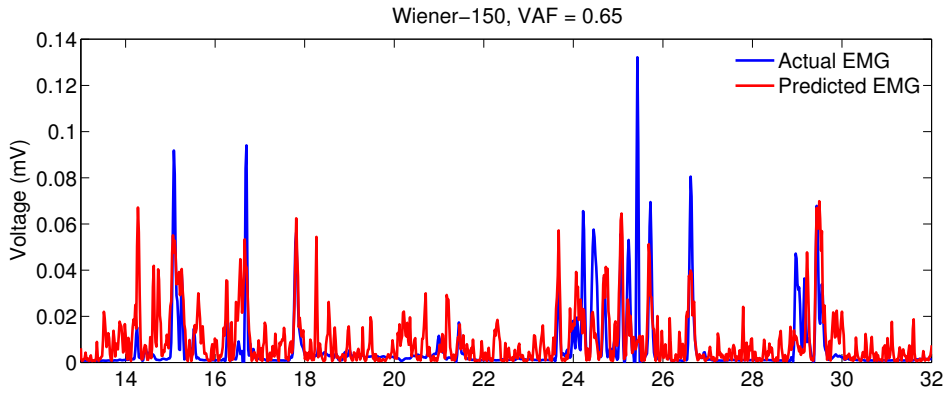

(a)

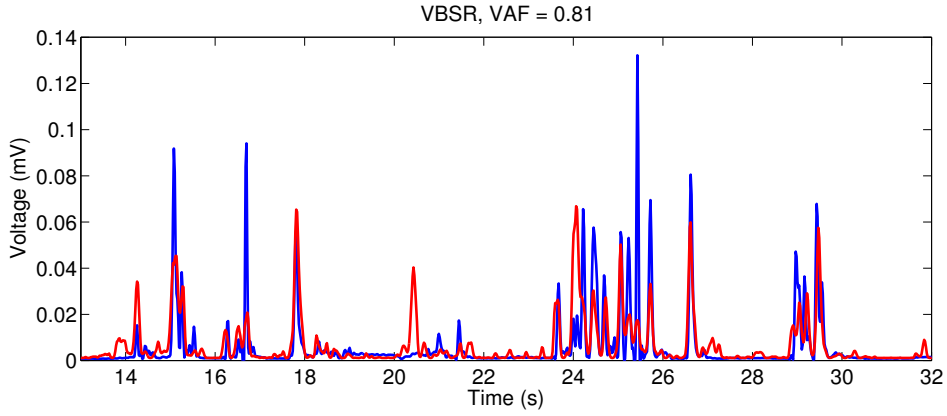

(b)

Figure 4.9: EMG prediction example for FCR muscle of datafile 'Block-241'. (*a*) Wiener-150 cascade model. (*b*) VBSR cascade model.

as the time required for fitting the models on 3 minutes of training data, are given in Table 4.3. For decoding, $N = 10$ bins were used, which yielded a total number of 3600 parameters. All analyses were performed on a 2.8 GHz Intel® Core i7 machine with 4 GB of memory, by using the MATLAB® environment. The most computationally expensive methods were LASSO/elastic net and ridge regression, due to the CV procedures required for parameter selection. Is it worth stressing that, although the VBSR algorithm requires more computational time than the Wiener cascade model during the training stage, it would be more suitable for real-time implementations, since by reducing the parameter space from 3600 to 1060 parameters on average, it requires less computational power during execution.

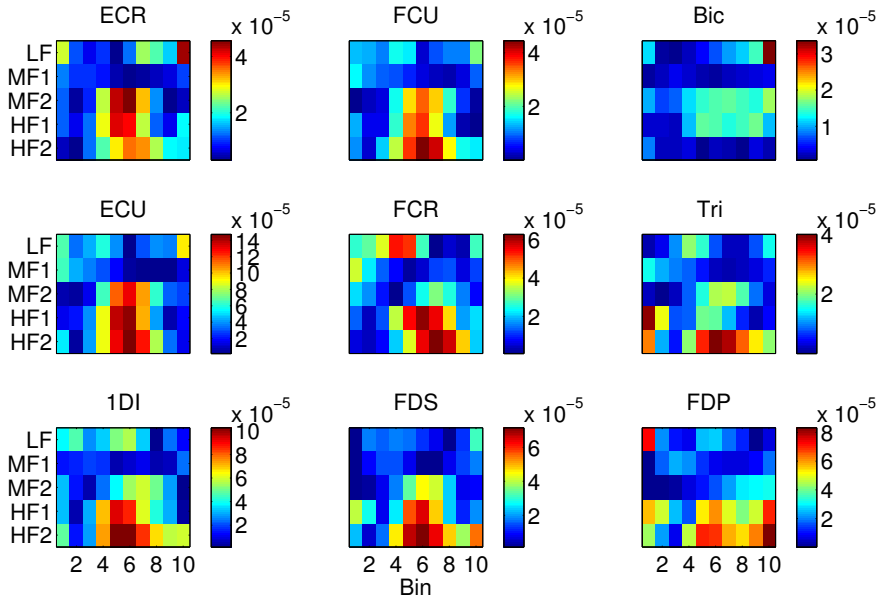

Figure 4.10: Variable selection with VBSR. Colour bars represent weight values assigned to input variables. Results shown for short (3 mins) training datasets. Data averaged across datafiles. Horizontal axis, time bins (length 51.2 ms); vertical axis, frequency bands, as in Section 3.4.1.

4.3.2 Variable selection with VBSR

In the previous section, it was shown that the VBSR algorithm yielded the best decoding performance with LFP signals. At this stage, we wish to evaluate the variable selection performed by the algorithm. In order to do so, we plotted the average weights assigned by the algorithm to the the input variables, and the results are shown in Fig. 4.10. In these plots, the horizontal axes represent the $N = 10$ time bins used for decoding, whereas the vertical axes represent the 5 LFP frequency bands. It can be easily observed that relatively larger weights were assigned to the high and mid-high LFP frequency components (i.e. MF2, H1 and H2 frequency bands). This is consistent with our findings in Section 4.2.1, where it was shown that these specific bands conveyed relatively more information about muscle activity, compared to the low and mid-low frequency bands (Table 4.1). Additionally, time bins 4-6, which correspond to time lags between 128 and 230 ms were favoured, which is also consistent with our findings in Section 4.1.1 (Fig. 4.3(b)).

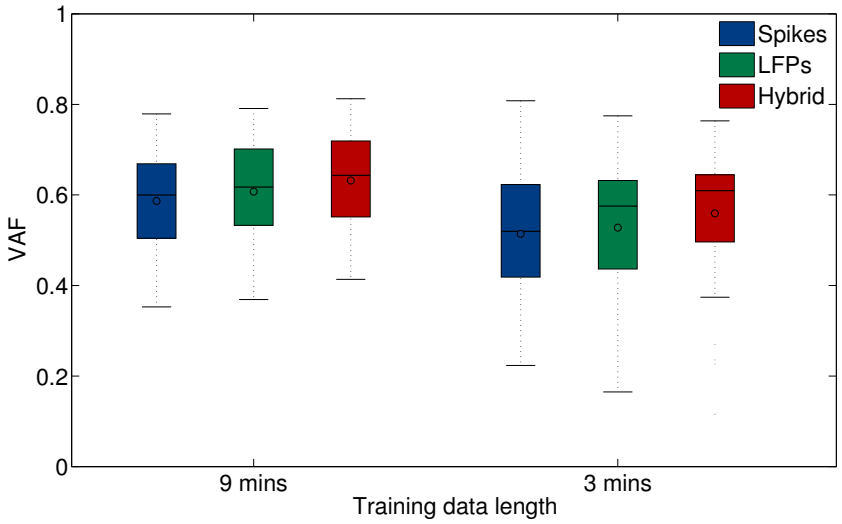

Figure 4.11: Source signal comparison for muscle activity prediction. For each type of decoder, the algorithm that yielded the best individual prediction was chosen. Data averaged across muscles and datafiles. Box symbols the same as in Fig. 4.2.

4.3.3 Source signal comparison

In the previous section, we showed that EMG prediction accuracy depended on the decoding algorithm, especially when the amount of available training data was limited. As a last step, we wished to compare the decoding performance of the three types of source signals (i.e. spikes, LFPs and hybrid signals), by using in each case the decoding algorithm which individually yielded the best performance in our comparison. The results, again for two different scenarios of training data availability, are shown in Fig. 4.11. The overall mean performance of the hybrid decoders was slightly higher than for spike- and LFP-decoders, however these differences were not significant ($P > 0.05$ for all comparisons; paired t-tests).

4.3.4 Remarks

In this section, we compared the EMG decoding performance of various regression techniques and found that for decoding with LFP signals, a variational Bayesian method outperformed the Wiener-150 cascade model when the amount of available training data was limited (Fig. 4.7(b), 4.9 and Table 4.2), however at the expense of additional computational cost during the training stage (Table 4.3). The VBSR method effectively reduced the parameter space from 3360 to an average of 1060 parameters, which prevented the produced models from overfitting the training data. The method

was successful in selecting the LFP components which were most informative of the EMG signals, both in frequency and time (Fig. 4.6, 4.3(b) and 4.10). For long training datafiles, the results were comparable between all methods. This was also the case for spike-decoders, since the number of parameters for this type of decoders was significantly smaller than for LFP- and hybrid decoders.

Finally, we compared the EMG prediction accuracy for different types of source signals, and found no significant differences between these decoders. Nevertheless, we found that by combining SA and LFP signals (i.e. hybrid decoders), the predictions were likely to be more robust, as suggested by the reduced standard deviation of the decoding accuracy shown in Fig. 4.11.

Chapter 5

Conclusions

In this final chapter, we summarise the most important findings of our study, and also reflect on future research directions.

5.1 Muscle activity decoding during free behaviour

We have shown that muscle activity in freely-behaving primates, as measured by EMG signals, can be decoded from cortical signals in M1 and PMv areas of the brain. The prediction accuracy of our decoders suggests that it would be feasible to effectively drive a FES system in a real-time environment. For comparison, Ethier et al. (2012) applied FES to monkeys whose forearms were previously paralysed by a peripheral nerve block, and demonstrated that the monkeys regained the ability to perform grasping tasks. In their study, the overall mean prediction accuracy across muscles and sessions was $R^2 = 0.58 \pm 0.12$, while the overall mean decoding performance of our models was $R^2 = 0.59 \pm 0.07$ for spike-, 0.58 ± 0.09 for LFP- and 0.61 ± 0.07 for hybrid decoders. To the best of our knowledge, this is the first study to clearly demonstrate that muscle activity prediction is feasible during naturalistic free behaviour. Some previous studies (Bansal et al., 2011, 2012; Zhuang et al., 2010), showed that it was possible to predict movement parameters during free behaviour, but they were limited to decoding kinematic parameters, such as hand position and velocity. Whether these predictions could be effective in reanimating paralysed upper limb muscles in primates yet remains to be tested, however, a basic behavioural task might be needed in that case, in order to assess the performance of EMG decoding and the FES system.

Our analyses were limited to data coming from a single animal, although data from a second animal were being collected at the Institute of Neuroscience, University of

Newcastle, at the time this manuscript was written. The methods presented in this work will be further tested when the data from the second animal become available. An aspect which was not considered in this work was whether muscle activity decoding can be generalised to different tasks. We plan to address this issue in the future, by training decoders on datafiles coming from free behaviour sessions, and testing their prediction accuracy during specific-task sessions. We believe that shedding light on this issue might be of significant importance to future real-life BMI applications.

5.2 Feature selection for muscle activity decoding from LFP signals and implications for BMIs

It has been already known that LFP signals recorded from M1 and PMv can be used to decode EMG activity of muscles from both the proximal and distal arm (Flint et al., 2012a). LFP signals could provide an alternative, or complementary, source signal for BMIs with numerous advantages compared to SA signals, such as greater longevity and lower sampling rate requirements, which translates into lower power consumption (Flint et al., 2012a; Linderman et al., 2008). Consistently with previous studies (Flint et al., 2012a; Bansal et al., 2011, 2012; Zhuang et al., 2010), we found that high and mid-high frequency bands (70-244 Hz) were the most movement-related informative signals. A future challenge will be to achieve equal decoding performance by only using low-frequency components of the LFP signals (Bansal et al., 2011), which will lead to even lower power requirements.

A caveat of the Wiener cascade model is that when the amount of training data is limited, it substantially suffers from overfitting. We found that a Variational Bayesian method outperformed the Wiener cascade model in this scenario, as the algorithm was successful in selecting a variant number of features which were most informative of the EMG signals. The ARD property of the VBSR method makes it particularly attractive, especially in future applications where the number of simultaneously recorded electrodes and, consequently, the number of input signals to the decoder are expected to increase dramatically. At the same time, the requirement for training data remains a challenge for clinical implementations of neural prosthetic systems with paralysed patients (Nazarpour et al., 2012). This, or any similar in nature algorithm, can be proven particularly useful in clinical applications, by training decoders at the early stages after implantation.

As a final note, we would like to stress that EMG prediction might be improved by reducing the dimensionality not only of the input, but also of the output of the system.

The Wiener cascade model treats the EMG decoding problem as a MISO system, rather than a single multiple-input-multiple-output (MIMO) system. Consequently, the correlations in the output of the system, i.e. the EMG signals, which are often very strong, are not exploited. We suspect that more accurate EMG predictions might emerge by projecting the output onto a lower-dimensional manifold, then make predictions on this subspace, and eventually backproject the data onto the original space. A possible way to approach this issue could be by making use of the muscle synergies hypothesis, which briefly suggests that the central nervous system (CNS) produces movement by combining a small number of predefined modules, called muscle synergies (D'Avella et al., 2003; Brochier et al., 2004; Miller, 2004; Alessandro et al., 2013). Additionally, there has been preliminary evidence that muscle synergies can form a predictive framework for EMG activity (Ajiboye and Weir, 2009). Further improvement in decoding performance might be also achieved by considering a set of hidden states in the model, which account for muscular fatigue, the subject's level of attention, or any other unobserved factors in the subject's environment (Lawhern et al., 2010; Wu et al., 2009).

5.3 Conclusion

In conclusion, we have shown that muscle activity in freely-behaving primates can be predicted from spikes and LFP signals from the motor cortices. The quality of EMG reconstruction, however, depends strongly on the selection of an appropriate decoding algorithm. Moving from laboratory setups to clinically viable solutions, requires overcoming a series of engineering challenges, which the research community is now ready to address.

Appendix A

Wiener-150 cascade model

A.1 EMG low-pass filter cutoff frequency

The mean overall decoding performance with the Wiener-150 cascade model is shown here, for two different cutoff frequencies of the digital filter used for the envelope extraction of EMG signals. In both cases, a 4th-order Butterworth filter was used (see Section 3.4.2), with cutoff frequencies at 5 Hz and 10 Hz, respectively.

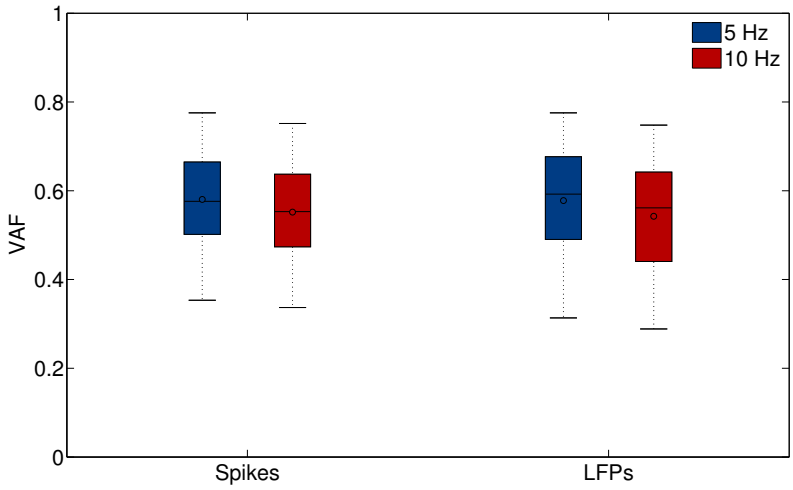

Figure A.1: Decoding performance with Wiener-150 cascade model for EMG low-pass cutoff frequencies of 5 and 10 Hz. Data averaged across muscles and datafiles. Box symbols the same as in Fig. 4.2.

A.2 Decoding performance for individual muscles

The decoding performance of the Wiener-150 cascade model for individual muscles and all three types of decoders is presented here. Mean results across muscles are shown in Fig. 4.2(a).

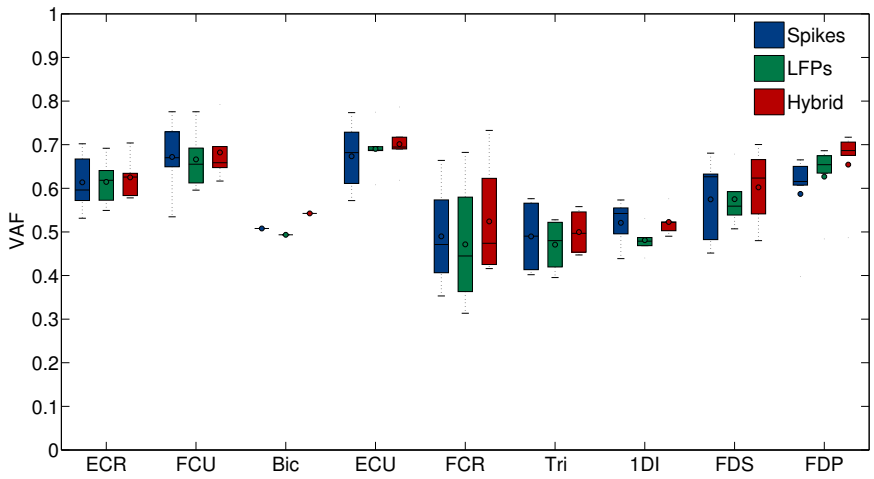

Figure A.2: Wiener-150 cascade model decoding performance for individual muscles. Results for long training datafiles are only shown. Data averaged across datafiles. For muscle 'Bic', only one recording was available. Box symbols the same as in Fig. 4.2.

A.3 M1 vs. PMv decoding

Here, we repeat the analysis described in Section 4.1.2, but without removing the additional LFP channels. In general, M1-decoders outperformed PMv-decoders (overall mean VAF $= 0.48 \pm 0.09$ vs. 0.28 ± 0.11, $P < 10^{-13}$ for spikes; 0.48 ± 0.10 vs. 0.46 ± 0.09, $P < 10^{-4}$ for LFPs; 0.61 ± 0.08 vs. 0.47 ± 0.09, $P < 10^{-13}$ for hybrid decoders).

For M1 signals, the hybrid decoder performed slightly better than spikes ($P < 0.05$), whereas it did not perform significantly better than LFPs ($P = 0.22$). The differences between spike- and LFP-decoders were not significant ($P = 0.30$). For PMv signals, both LFP- and hybrid decoders outperformed spikes ($P < 10^{-6}$ and $P < 10^{-7}$, respectively). The differences between the LFP- and hybrid decoders were not significant ($P = 0.47$).

Decoding performance for individual muscles are shown in Fig. A.4. The data shown

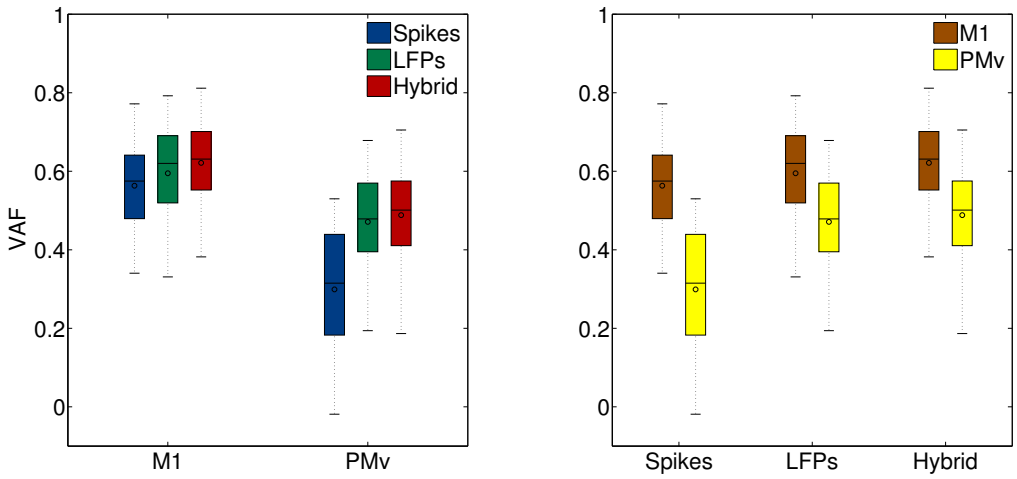

(a) (b)

Figure A.3: M1 vs. PMv decoding with Wiener-150 cascade model. (*a*) Performance comparison for different types of decoders in M1 and PMv, separately. (*b*) Performance comparison for same type of decoders between M1 and PMv. Results for long training datafiles are only shown. Data averaged across muscles and datafiles. Box symbols the same as in Fig. 4.2.

are averaged across datafiles, except for muscle 'Bic', for which only one recording session was available.

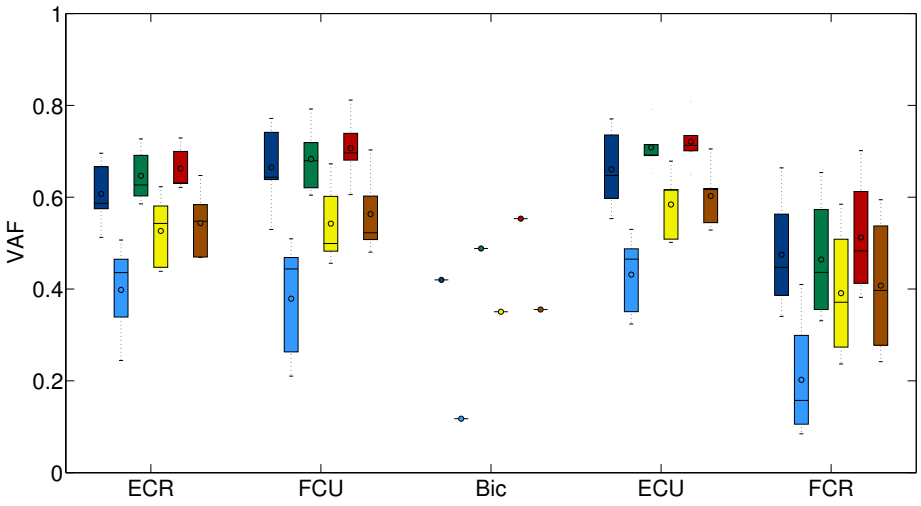

(a)

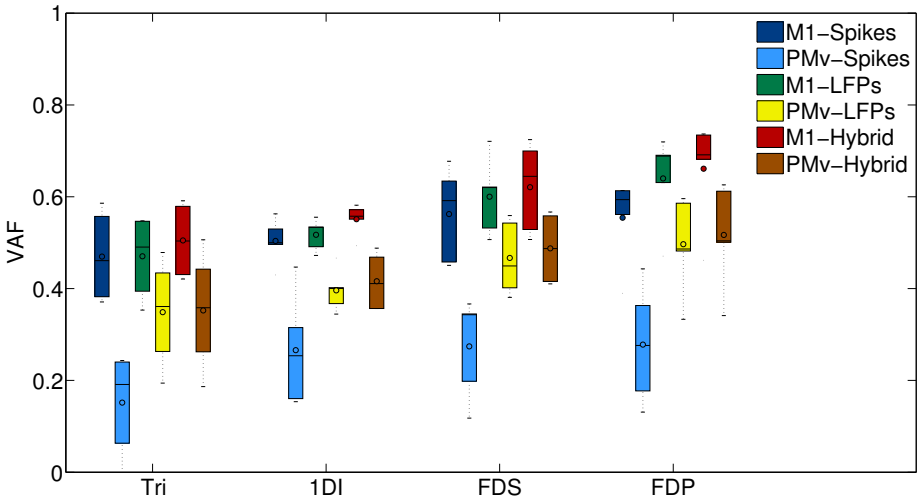

(b)

Figure A.4: M1 vs. PMv decoding with Wiener-150 cascade model for individual muscles. Data averaged across datafiles. For muscle 'Bic' data from only one recording session were available. Box symbols the same as in Fig. 4.2.

Appendix B

Wiener cascade model

B.1 Relative information in LFP frequency bands for individual muscles

In this section, the decoding performance of Wiener cascade decoders trained on single frequency bands (or the LMP), is shown for individual muscles. The mean results over muscles are presented in Fig. 4.6 and Table 4.1.

Additionally, example EMG predictions from different frequency bands for a 10-sec segment of activity of the FDP muscle, are shown in Fig. B.2.

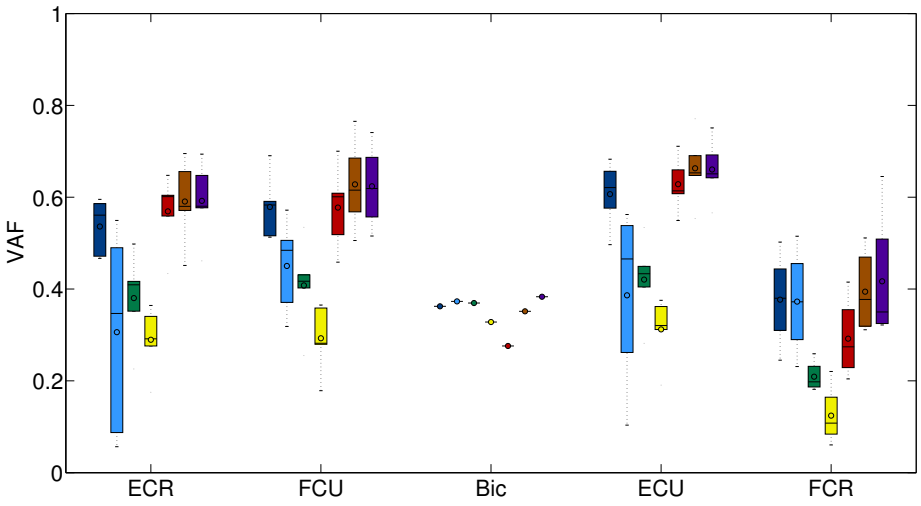

(a)

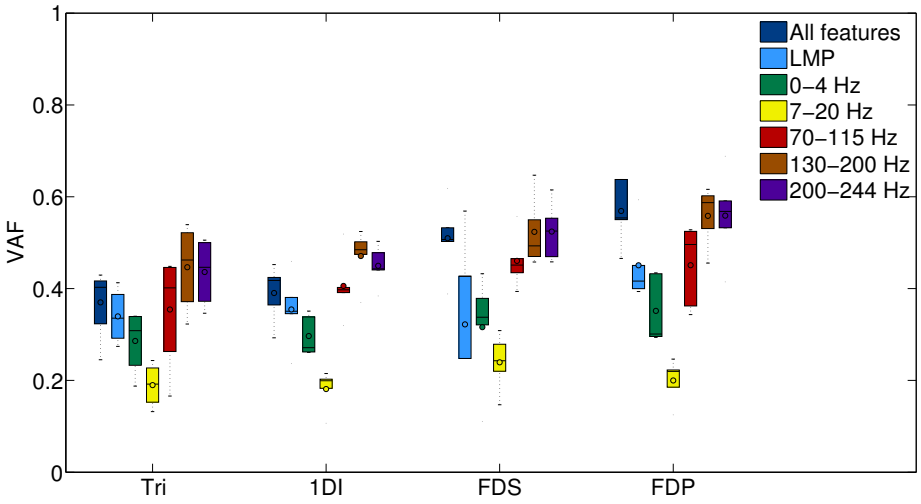

(b)

Figure B.1: Single-frequency band decoding performance with Wiener cascade model for individual muscles. For muscle 'Bic', only one recording was available. Box symbols the same as in Fig. 4.2.

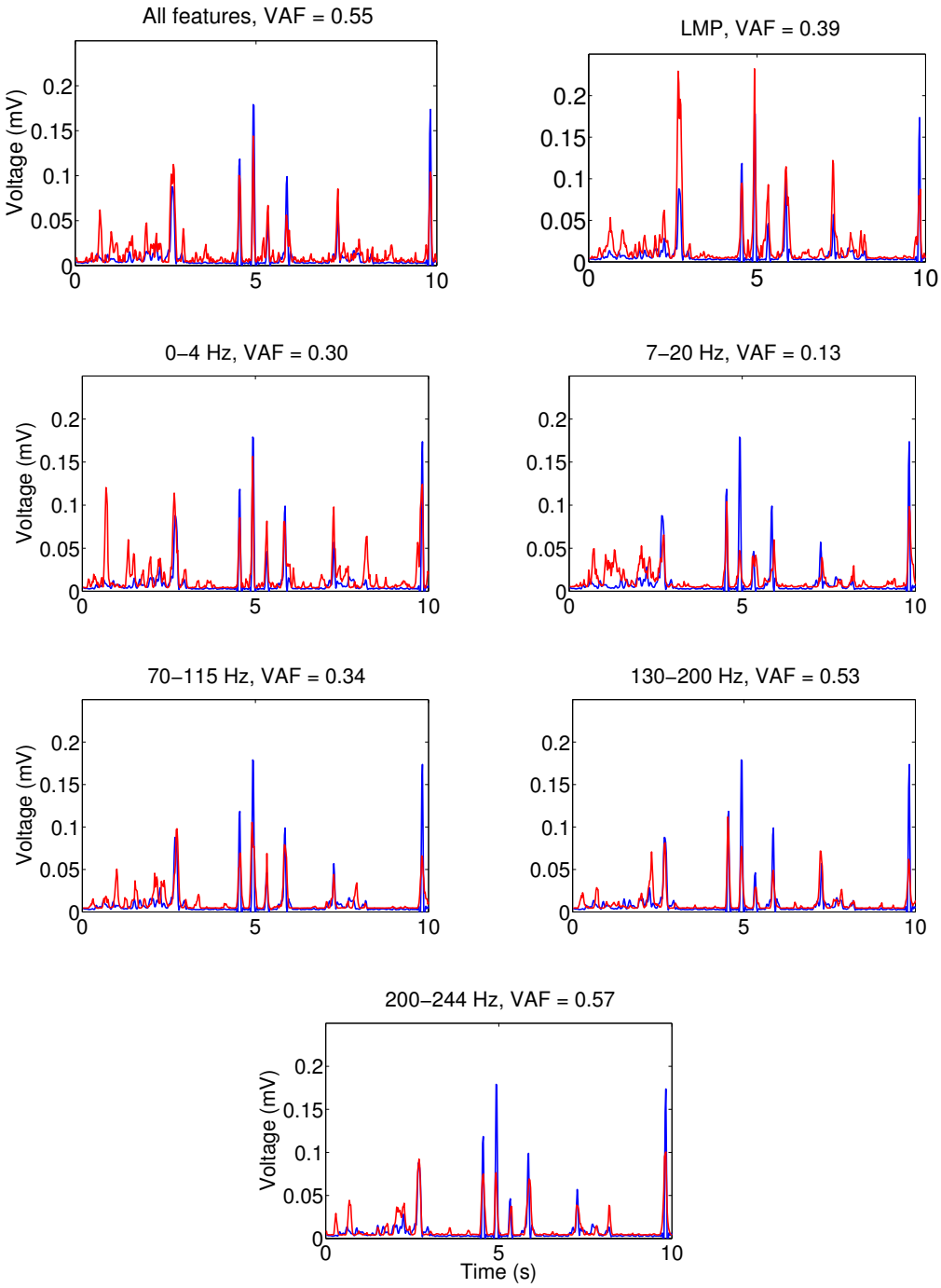

Figure B.2: Example EMG predictions with single-frequency bands for muscle 'FDP' and datafile 'Block-57'.

Appendix C

LASSO/elastic net

C.1 Comparison of LASSO and elastic net

In this section, we present a comparison of the decoding performance of LASSO and elastic net, for spike- and LFP-decoders, and show that they produce very similar predictions. The two algorithms yielded very similar results in both cases ($P = 0.99$ for spikes; $P = 0.62$ for LFPs; paired t-tests).

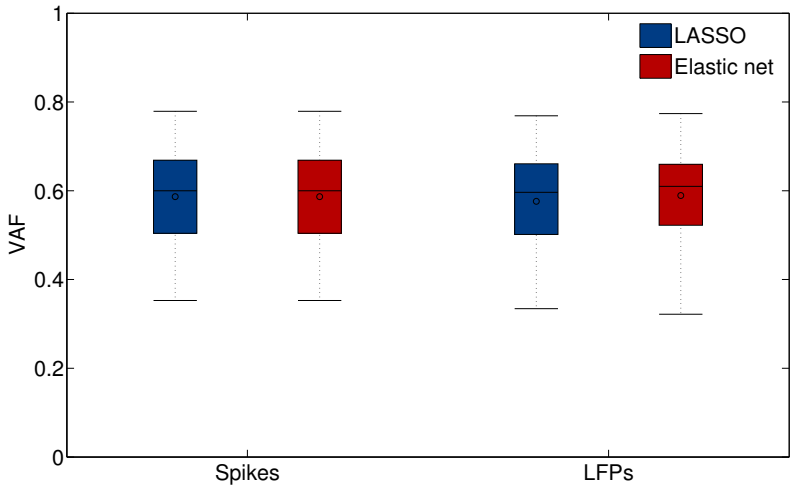

Figure C.1: Comparison of decoding performance between LASSO and elastic net. Data averaged across muscles and datafiles. Box symbols the same as in Fig. 4.2.

C.2 Variable selection with LASSO/elastic net

In this section, we evaluate the variable selection performed by LASSO/elastic net. For large training datasets (Fig. C.2(a)), larger values were assigned to the high and mid-high LFP frequency components, which conveyed more information about muscle activity than the low and mid-low frequency bands (Table 4.1 and Fig. 4.6). On the other hand, for short training datasets, this selectivity was less obvious (Fig. C.2(b)), which might explain the poor performance of the algorithm in that case.

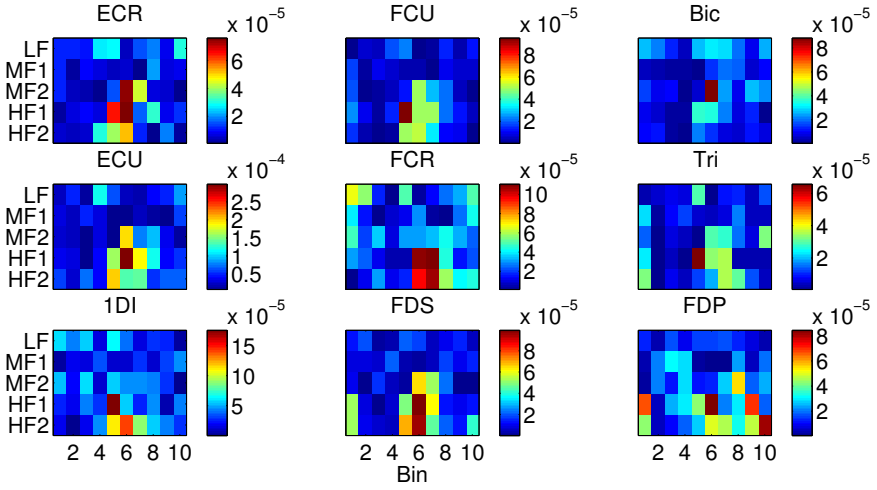

(a)

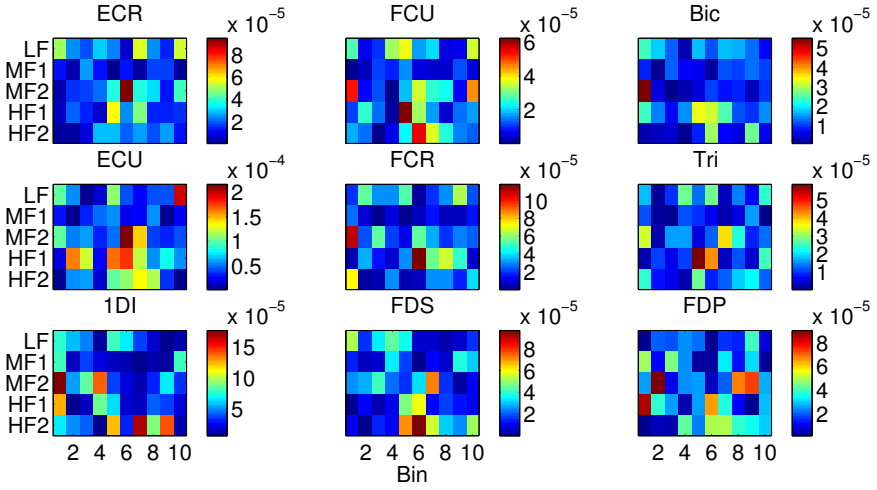

(b)

Figure C.2: Variable selection with LASSO/elastic net. Colour bars represent weight values assigned to input variables. Results shown for 9 mins (*a*) and 3 mins (*b*) of training data. Data averaged across datafiles. Horizontal axis, time bins (length 51.2 ms); vertical axis, frequency bands, as in Section 3.4.1.

Bibliography

A. P. Georgopoulos, J. F. Kalaska, R. Caminiti, J. T. Massey (1982). On the relations between the direction of two-dimensional arm movements and cell discharge in primate motor cortex. *The Journal of neuroscience: the official journal of the Society for Neuroscience*, 2(11):1527–37.

Ajiboye, A. B. and Weir, R. F. (2009). Muscle synergies as a predictive framework for the EMG patterns of new hand postures. *Journal of neural engineering*, 6(3):036004.

Alessandro, C., Delis, I., Nori, F., Panzeri, S., and Berret, B. (2013). Muscle synergies in neuroscience and robotics: from input-space to task-space perspectives. *Frontiers in computational neuroscience*, 7(April):43.

Asher, I., Stark, E., Abeles, M., and Prut, Y. (2007). Comparison of direction and object selectivity of local field potentials and single units in macaque posterior parietal cortex during prehension. *Journal of neurophysiology*, 97(5):3684–95.

Bansal, A. K., Truccolo, W., Vargas-Irwin, C. E., and Donoghue, J. P. (2012). Decoding 3D reach and grasp from hybrid signals in motor and premotor cortices: spikes, multiunit activity, and local field potentials. *Journal of neurophysiology*, 107(5):1337–55.

Bansal, A. K., Vargas-Irwin, C. E., Truccolo, W., and Donoghue, J. P. (2011). Relationships among low-frequency local field potentials, spiking activity, and three-dimensional reach and grasp kinematics in primary motor and ventral premotor cortices. *Journal of neurophysiology*, 105(4):1603–19.

Bishop, C. M. (2006). *Pattern Recognition and Machine Learning (Information Science and Statistics)*. Springer-Verlag New York, Inc., Secaucus, NJ, USA.

Brochier, T., Spinks, R. L., Umilta, M. a., and Lemon, R. N. (2004). Patterns of muscle activity underlying object-specific grasp by the macaque monkey. *Journal of neurophysiology*, 92(3):1770–82.

Buzsáki, G. (2004). Large-scale recording of neuronal ensembles. *Nature neuroscience*, 7(5):446–51.

Carmena, J. M., Lebedev, M. A., Crist, R. E., O'Doherty, J. E., Santucci, D. M., Dimitrov, D. F., Patil, P. G., Henriquez, C. S., and Nicolelis, M. A. L. (2003). Learning to control a brain-machine interface for reaching and grasping by primates. *PLoS biology*, 1(2):E42.

Chao, Z. C., Nagasaka, Y., and Fujii, N. (2010). Long-term asynchronous decoding of arm motion using electrocorticographic signals in monkeys. *Frontiers in neuroengineering*, 3(March):3.

Collinger, J. L., Wodlinger, B., Downey, J. E., Wang, W., Tyler-Kabara, E. C., Weber, D. J., McMorland, A. J. C., Velliste, M., Boninger, M. L., and Schwartz, A. B. (2013). High-performance neuroprosthetic control by an individual with tetraplegia. *Lancet*, 381(9866):557–64.

D'Avella, A., Saltiel, P., and Bizzi, E. (2003). Combinations of muscle synergies in the construction of a natural motor behavior. *Nature neuroscience*, 6(3):300–8.

Ethier, C., Oby, E. R., Bauman, M. J., and Miller, L. E. (2012). Restoration of grasp following paralysis through brain-controlled stimulation of muscles. *Nature*, 485(7398):368–71.

Evarts, E. V. (1968). Relation of pyramidal tract activity to force exerted during voluntary movement. *Journal of neurophysiology*, 31(1):14–27.

Flint, R. D., Ethier, C., Oby, E. R., Miller, L. E., and Slutzky, M. W. (2012a). Local field potentials allow accurate decoding of muscle activity. *Journal of neurophysiology*, 108(1):18–24.

Flint, R. D., Lindberg, E. W., Jordan, L. R., Miller, L. E., and Slutzky, M. W. (2012b). Accurate decoding of reaching movements from field potentials in the absence of spikes. *Journal of neural engineering*, 9(4):046006.

Gilja, V., Nuyujukian, P., Chestek, C. a., Cunningham, J. P., Yu, B. M., Fan, J. M., Churchland, M. M., Kaufman, M. T., Kao, J. C., Ryu, S. I., and Shenoy, K. V. (2012). A high-performance neural prosthesis enabled by control algorithm design. *Nature neuroscience*, 15(12):1752–7.

Heldman, D. A., Wang, W., Chan, S. S., and Moran, D. W. (2006). Local field potential spectral tuning in motor cortex during reaching. *IEEE transactions on neural systems*

and rehabilitation engineering : a publication of the IEEE Engineering in Medicine and Biology Society, 14(2):180–3.

Hochberg, L. R., Bacher, D., Jarosiewicz, B., Masse, N. Y., Simeral, J. D., Vogel, J., Haddadin, S., Liu, J., Cash, S. S., van der Smagt, P., and Donoghue, J. P. (2012). Reach and grasp by people with tetraplegia using a neurally controlled robotic arm. *Nature*, 485(7398):372–5.

Hochberg, L. R., Serruya, M. D., Friehs, G. M., Mukand, J. a., Saleh, M., Caplan, A. H., Branner, A., Chen, D., Penn, R. D., and Donoghue, J. P. (2006). Neuronal ensemble control of prosthetic devices by a human with tetraplegia. *Nature*, 442(7099):164–71.

Hwang, E. J. and Andersen, R. a. (2013). The utility of multichannel local field potentials for brain-machine interfaces. *Journal of neural engineering*, 10(4):046005.

Jackson, A. and Fetz, E. E. (2007). Compact movable microwire array for long-term chronic unit recording in cerebral cortex of primates. *Journal of neurophysiology*, 98(5):3109–18.

Lawhern, V., Wu, W., Hatsopoulos, N., and Paninski, L. (2010). Population decoding of motor cortical activity using a generalized linear model with hidden states. *Journal of neuroscience methods*, 189(2):267–80.

Linderman, M., Santhanam, G., Kemere, C., Gilja, V., O'Driscoll, S., Yu, B., Afshar, A., Ryu, S., Shenoy, K., and Meng, T. (2008). Signal Processing Challenges for Neural Prostheses. *IEEE Signal Processing Magazine*, 25(1):18–28.

Logothetis, N. K. (2002). The neural basis of the blood-oxygen-level-dependent functional magnetic resonance imaging signal. *Philosophical transactions of the Royal Society of London. Series B, Biological sciences*, 357(1424):1003–37.

Mehring, C., Rickert, J., Vaadia, E., Cardosa de Oliveira, S., Aertsen, A., and Rotter, S. (2003). Inference of hand movements from local field potentials in monkey motor cortex. *Nature neuroscience*, 6(12):1253–4.

Miller, L. E. (2004). Limb movement: getting a handle on grasp. *Current biology : CB*, 14(17):R714–5.

Mitzdorf, U. (1987). Properties of the evoked potential generators: Current source-density analysis of visually evoked potentials in the cat cortex. *International Journal of Neuroscience*, 33(1):33.

Moritz, C. T., Perlmutter, S. I., and Fetz, E. E. (2008). Direct control of paralysed muscles by cortical neurons. *Nature*, 456(7222):639–42.

Murthy, V. N. and Fetz, E. E. (1996). Oscillatory activity in sensorimotor cortex of awake monkeys: synchronization of local field potentials and relation to behavior. *Journal of neurophysiology*, 76(6):3949–67.

Nazarpour, K., Ethier, C., Paninski, L., Rebesco, J. M., Miall, R. C., and Miller, L. E. (2012). EMG prediction from motor cortical recordings via a nonnegative point-process filter. *IEEE transactions on bio-medical engineering*, 59(7):1829–38.

Oby, E. R., Ethier, C., and Miller, L. E. (2013). Movement representation in the primary motor cortex and its contribution to generalizable EMG predictions. *Journal of neurophysiology*, 109(3):666–78.

Perreault, E. J., Kirsch, R. F., and Acosta, A. M. (1999). Multiple-input, multiple-output system identification for characterization of limb stiffness dynamics. *Biological cybernetics*, 80(5):327–37.

Pistohl, T., Ball, T., Schulze-Bonhage, A., Aertsen, A., and Mehring, C. (2008). Prediction of arm movement trajectories from ECoG-recordings in humans. *Journal of neuroscience methods*, 167(1):105–14.

Pohlmeyer, E. A., Solla, S. A., Perreault, E. J., and Miller, L. E. (2007). Prediction of upper limb muscle activity from motor cortical discharge during reaching. *Journal of neural engineering*, 4(4):369–79.

Ray, S., Crone, N. E., Niebur, E., Franaszczuk, P. J., and Hsiao, S. S. (2008). Neural correlates of high-gamma oscillations (60-200 Hz) in macaque local field potentials and their potential implications in electrocorticography. *The Journal of neuroscience: the official journal of the Society for Neuroscience*, 28(45):11526–36.

Rickert, J., de Oliveira, S. C., Vaadia, E., Aertsen, A., Rotter, S., and Mehring, C. (2005). Encoding of movement direction in different frequency ranges of motor cortical local field potentials. *The Journal of neuroscience: the official journal of the Society for Neuroscience*, 25(39):8815–24.

Sanchez, J. C., Gunduz, A., Carney, P. R., and Principe, J. C. (2008). Extraction and localization of mesoscopic motor control signals for human ECoG neuroprosthetics. *Journal of neuroscience methods*, 167(1):63–81.

Sanes, J. N. and Donoghue, J. P. (1993). Oscillations in local field potentials of the primate motor cortex during voluntary movement. *Proceedings of the National Academy of Sciences*, 90(10):4470–4474.

Sato, M. (2001). Online Model Selection Based on the Variational Bayes. *Neural Computation*, 13(7):1649–1681.

Schalk, G., Kubánek, J., Miller, K. J., Anderson, N. R., Leuthardt, E. C., Ojemann, J. G., Limbrick, D., Moran, D., Gerhardt, L. a., and Wolpaw, J. R. (2007). Decoding two-dimensional movement trajectories using electrocorticographic signals in humans. *Journal of neural engineering*, 4(3):264–75.

Scherberger, H., Jarvis, M. R., and Andersen, R. a. (2005). Cortical local field potential encodes movement intentions in the posterior parietal cortex. *Neuron*, 46(2):347–54.

Serruya, M. D., Hatsopoulos, N. G., Paninski, L., Fellows, M. R., and Donoghue, J. P. (2002). Instant neural control of a movement signal. *Nature*, 416(6877):141–2.

Shimoda, K., Nagasaka, Y., Chao, Z. C., and Fujii, N. (2012). Decoding continuous three-dimensional hand trajectories from epidural electrocorticographic signals in Japanese macaques. *Journal of neural engineering*, 9(3):036015.

Shin, D., Watanabe, H., Kambara, H., Nambu, A., Isa, T., Nishimura, Y., and Koike, Y. (2012). Prediction of muscle activities from electrocorticograms in primary motor cortex of primates. *PloS one*, 7(10):e47992.

Simeral, J. D., Kim, S.-P., Black, M. J., Donoghue, J. P., and Hochberg, L. R. (2011). Neural control of cursor trajectory and click by a human with tetraplegia 1000 days after implant of an intracortical microelectrode array. *Journal of neural engineering*, 8(2):025027.

Slutzky, M. W., Jordan, L. R., Lindberg, E. W., Lindsay, K. E., and Miller, L. E. (2011). Decoding the rat forelimb movement direction from epidural and intracortical field potentials. *Journal of neural engineering*, 8(3):036013.

Spinks, R. L., Kraskov, A., Brochier, T., Umilta, M. A., and Lemon, R. N. (2008). Selectivity for grasp in local field potential and single neuron activity recorded simultaneously from M1 and F5 in the awake macaque monkey. *The Journal of neuroscience : the official journal of the Society for Neuroscience*, 28(43):10961–71.

Stark, E. and Abeles, M. (2007). Predicting movement from multiunit activity. *The Journal of neuroscience : the official journal of the Society for Neuroscience*, 27(31):8387–94.

Tibshirani, R. (2011). Regression shrinkage and selection via the lasso: a retrospective. *Journal of the Royal Statistical Society: Series B (Statistical Methodology)*, 73(3):273–282.

Tikhonov, A. (1943). On the stability of inverse problems. *Doklady Akademii nauk SSSR*, 39(5):195–198.

Ting, J.-A., D'Souza, A., Vijayakumar, S., and Schaal, S. (2010). Efficient learning and feature selection in high-dimensional regression. *Neural computation*, 22(4):831–86.

Velliste, M., Perel, S., Spalding, M. C., Whitford, A. S., and Schwartz, A. B. (2008). Cortical control of a prosthetic arm for self-feeding. *Nature*, 453(7198):1098–101.

Westwick, D. T., Pohlmeyer, E. A., Solla, S. A., Miller, L. E., and Perreault, E. J. (2006). Identification of multiple-input systems with highly coupled inputs: application to EMG prediction from multiple intracortical electrodes. *Neural computation*, 18(2):329–55.

Wu, W., Gao, Y., Bienenstock, E., Donoghue, J. P., and Black, M. J. (2006). Bayesian population decoding of motor cortical activity using a Kalman filter. *Neural computation*, 18(1):80–118.

Wu, W., Kulkarni, J. E., Hatsopoulos, N. G., and Paninski, L. (2009). Neural decoding of hand motion using a linear state-space model with hidden states. *IEEE transactions on neural systems and rehabilitation engineering : a publication of the IEEE Engineering in Medicine and Biology Society*, 17(4):370–8.

Zhuang, J., Truccolo, W., Vargas-Irwin, C., and Donoghue, J. P. (2010). Decoding 3-D reach and grasp kinematics from high-frequency local field potentials in primate primary motor cortex. *IEEE transactions on bio-medical engineering*, 57(7):1774–84.

Zou, H. and Hastie, T. (2005). Regularization and variable selection via the elastic net. *Journal of the Royal Statistical Society: Series B (Statistical Methodology)*, 67(2):301–320.